Biochimica et Biophysica Acta 1817 (2012) 106–120

Contents lists available at ScienceDirect

Biochimica et Biophysica Acta

journal homepage: www.elsevier.com/locate/bbabio

Review

Structural and mechanistic investigations of photosystem II through computational methods☆

Felix M. Ho *

Molecular Biomimetics, Department of Photochemistry and Molecular Science, Ångström Laboratory, Uppsala University, P.O. Box 523, SE-751 20 Uppsala, Sweden

ARTICLE INFO

Article history:
Received 25 January 2011
Received in revised form 22 March 2011
Accepted 2 April 2011
Available online 1 May 2011

Keywords:
Photosystem II
Water oxidation
Channels
Simulation
Computation

ABSTRACT

The advent of oxygenic photosynthesis through water oxidation by photosystem II (PSII) transformed the planet, ultimately allowing the evolution of aerobic respiration and an explosion of ecological diversity. The importance of this enzyme to life on Earth has ironically been paralleled by the elusiveness of a detailed understanding of its precise catalytic mechanism. Computational investigations have in recent years provided more and more insights into the structural and mechanistic details that underlie the workings of PSII. This review will present an overview of some of these studies, focusing on those that have aimed at elucidating the mechanism of water oxidation at the $CaMn_4$ cluster in PSII, and those exploring the features of the structure and dynamics of this enzyme that enable it to catalyse this energetically demanding reaction. This article is part of a Special Issue entitled: Photosystem II.

1. Introduction

As the enzyme that first enabled oxygenic photosynthesis to take place around 2.5 million years ago, photosystem II (PSII) has transformed life on Earth, enabling an explosion of ecological diversity that was impossible before the evolution of aerobic respiration. The ability of PSII to harness light energy to accumulate sufficient oxidation potential at the oxygen-evolving complex (OEC) to split water under mild physiological conditions is remarkable to say the least. Yet, despite the enzyme's vital and fundamental importance, structural and mechanistic information about PSII has proven to be most elusive. Attempts to obtain a high-quality X-ray crystal structure of PSII were hampered by difficulties in crystallising this large multi-subunit transmembrane protein complex, as well as the susceptibility of the crucial $CaMn_4$ metal cluster of the OEC to radiation damage upon exposure to X-ray radiation during measurements [1]. Only in recent years have fully refined medium-resolution (2.9–3.5 Å) crystal structures become available, obtained from the thermophilic cyanobacterium *Thermosynchoccocus elongatus*[2–4], and the announcement of a 1.9 Å-resolution structure obtained from *Thermosynechococcus vulcanus* showing the enzyme in atomic detail was greeted with a standing ovation at the 2010 15th International Photosynthesis Congress in Beijing. This structure has very recently been published (see Note added in proof). Nevertheless, despite a lack of crystallographic data, a myriad of biochemical and spectroscopic methods have been used to try to unlock the mysteries surrounding the mechanism by which PSII is able to oxidise water (see reviews in [5,6]).

In addition to these experimental investigations, computational studies have also sought to increase our understanding of the workings of PSII. The earliest structural studies were based on the sequence homologies that were found between the core D1 and D2 subunits of PSII, and the L and M subunits of the bacterial reaction centre from the purple bacteria *Rhodopseudomonas viridis* and *Rhodobacter sphaerodies*, for which crystal structures were available [7–12]. Apart from deducing the secondary and tertiary structures of the D1 and D2 subunits, these studies predicted with remarkable accuracy, given the available information, the positions and orientations of the redox-active amino acid Y_Z, Y_D (the origin of the so-called long-lived tyrosine signal Signal II_{slow}), the binding sites of the various co-factors, and the $CaMn_4$ cluster. This was achieved by a combination of homology structure building against the bacterial reaction centres, both with and without "knowledge-based" searching of other known structures of similar sequences, references to and simulations of a range of literature spectroscopic data, as well as energy minimisation calculations. Although not always correct in every aspect, many of these predictions have been borne out by subsequent experiments, and these studies provided substantial insights into the structure and mechanism of PSII at a time when structure information was still limited.

Abbreviations: Chl, chlorophyll; DFT, density functional theory; EPR, electron paramagnetic resonance; ESEEM, electron spin echo envelope modulation; ESP, electrostatic potential; EXAFS, extended X-ray absorption fine structure; FT-IR, Fourier transform infra-red; HF, Hartree–Fock; OEC, oxygen-evolving complex; MD, molecular dynamics; MEP, minimum energy path; MM, molecular mechanics; P_{680}, the primary donor in PSII; PSII, photosystem II; Q_A and Q_B, the primary and secondary quinone acceptors in PSII, respectively; QM, quantum mechanics; Y_D, tyrosine 161 of the PSII D2 polypeptide; Y_Z, tyrosine 161 of the PSII D1 polypeptide

☆ This article is part of a Special Issue entitled: Photosystem II.

* Tel.: +46 18 471 6584; fax: +46 18 471 6844.
E-mail address: Felix.Ho@fotomol.uu.se.

0005-2728/$ – see front matter © 2011 Elsevier B.V. All rights reserved.
doi:10.1016/j.bbabio.2011.04.009

Fast forward 20 years, and the availability of crystallographic data as well as the enormous improvements in computing power have greatly expanded the possibilities to study the structure and function of PSII in greater detail with the help of simulations and calculations. This short review will focus mainly on recent computational investigations of two aspects associated with water oxidation in PSII, namely, the detailed molecular mechanism of the S-cycle of the $CaMn_4$ cluster, and the identification and assignment of channels in PSII for the transport of substrates and products to and from the cluster. This will be followed by a brief overview of a few other computational studies related to the structural characteristics and dynamics of PSII.

2. Mechanism of water oxidation at the OEC

Of central importance to the study of PSII is the mechanism of water oxidation at the OEC. While it is known that for each water oxidation event the $CaMn_4$ cluster undergoes transitions through five intermediates (S_0 to S_4) in the S-cycle, the precise mechanistic details such as the sites of oxidation, deprotonation and water binding, changes in the structure of the cluster during the S-cycle, and crucially the mechanism of the O—O bond formation step are still not fully understood. Experimental efforts using techniques such as EPR, FT-IR and EXAFS spectroscopies continue to provide more and more insight into these details, but much remains unknown and under debate (see [13] for a review).

A major challenge for all such mechanistic studies of water oxidation, both experimental and computational, has been the lack of definitive structures of the OEC during each step of the S-cycle. Until very recently, the PSII X-ray crystal structures available did not have high enough resolution to give detailed assignments of the position of the individual atoms in the cluster [2–4], and as mentioned above, it seems likely that the structures obtained have been affected by radiation damage during measurements [1]. While recent high-quality EXAFS studies (both isotropic [14,15] and polarised EXAFS [16]) have significantly narrowed down the number of possible structural candidates, uncertainty remains. The new crystal structure at 1.9 Å resolution (PDB ID: 3ARC) provides an atomic resolution view of the cluster in the S_1-state. Nevertheless, questions remain for the remaining S states, and there is indication that some degree of Mn-reduction may have taken place even in this structure (though to a very substantially lower extent than for the previous structures). Furthermore, the electronic structure of the cluster during the S-cycle is also under intense discussion between the Berlin [13] and Berkeley [17] EXAFS groups. As yet it is not clear which of the Mn ions are oxidised during S-state transitions, whether Mn-centred oxidation takes place in all steps, or what the nature of the structural rearrangement observed in the $S_2 \rightarrow S_3$ transition is.

A number of computational studies have in recent years tried to solve this mechanistic puzzle. Density functional theory (DFT) has been the quantum mechanical (QM) method of choice for calculating the energetic, geometric and magnetic properties of the $CaMn_4$ cluster and its ligands. DFT is a quantum mechanical method where the ground-state electronic energy and other properties of a system are taken to correspond uniquely to the system's ground-state electron density distribution, i.e. the energy of the system is a functional of $\rho(\mathbf{r})$, the electron density at a given point $\mathbf{r}$ in space. As such, it is not necessary to treat each electron individually. This increases the size of the systems that are amenable to calculations compared to Hartree–Fock (HF) methods. Additionally, DFT takes into account electron correlation effects between electrons which the HF method does not. However, the accuracy of the DFT calculations is sensitive to the form that the functional used for the energy calculations takes, and the formulation of a satisfactory expression for exchange-correlation energy is a very challenging aspect of functional development. (For more detailed overviews of DFT and functionals see [18,19].)

Two different computational approaches have been used to study the water oxidation mechanism. Although they share the common feature of treating the OEC using DFT, different methods have been used to account for the remainder of the PSII complex. More importantly, conceptually different methodologies and criteria have been used to arrive at their respective proposals for the water oxidation mechanism. These are reviewed in turn below. For each approach, an overview of the methodology and protocol used for the computation is first presented (Sections 2.1.1 and 2.2.1), followed by summaries of the results obtained using each approach for elucidating the S-state cycle (Sections 2.1.2 and 2.2.2). Readers more interested in the computational results from these different approaches may wish to proceed directly to Sections 2.1.2 and 2.2.2. An evaluation of the methods used and their implications for the results obtained are presented in Section 2.3.

2.1. Cluster model approach with DFT

2.1.1. Methodology—cluster model DFT

In a long line of studies spanning over a decade [20–32], Siegbahn and co-workers have performed DFT calculations using a cluster model approach. In this method, a cluster consisting of the $CaMn_4$ cluster and a number of atoms from the surrounding ligands are explicitly considered, with the polarisation of the remaining protein medium being approximated by the inclusion of a constant dielectric. Starting from a total of around 30–40 atoms at a time when structural information about the cluster and the surrounding was very limited [20,21], the most recent calculations have expanded to cluster models of around 200 atoms that include the $CaMn_4$ cluster, the full ligand sphere, a second-shell ligand (CP43-R357) some water molecules and a chloride ion (Fig. 1A) [26,30,32]. The positions of the ligand backbone atoms are taken from the London crystal structure (PDB ID: 1S5L, 3.5 Å [2]), and the ligand motifs for the sidechains are akin to those found in the Berlin crystal structure (PDB ID: 2AXT, 3.0 Å [3]).

A key feature of the work by Siegbahn and co-workers is the focus on the energetics of all structural intermediates and mechanistic pathways that have been proposed for the S-cycle. Two central criteria for discriminating between the vast array of possible structures and mechanisms can be discerned from these studies.

The first criterion is that, whatever the intermediate structures in the cycle may be, they must lead to a low barrier O—O formation step with an energy barrier that fits with the millisecond kinetics for O_2 formation (13–14 kcal/mol as estimated from transition state theory). This was the focus of the earlier studies, and extensive studies were made to identify the most favourable mechanism for O—O bond formation, as well as the geometries within the cluster in the S_4 state that would be required to allow this to take place [20,21,24,25]. It was found that nucleophilic attack on an oxygen radical bound to a Mn^{IV} ion in the cluster gave the most energetically favourable mechanism. Initial work had suggested an attack on a Mn^{IV}–$O^{\bullet}$ radical by an external substrate molecule [20]. However, exhaustive studies of thousands of possible structures of the S_4 state and several different mechanisms [24,25] subsequently showed that in fact an attack by a μ-oxo bridge oxygen on such a radical oxygen species led to a much more reasonable energy barrier.

The studies of different spin configurations on the O and Mn atoms involved also revealed an additional spin alignment requirement for a low barrier O—O formation mechanism (Fig. 1B). In order to form the O—O bond, the oxygen atoms involved must have opposite spins. For the lowest barrier mechanism, the Mn atoms must also have opposite spins to their respective bound oxygen atoms. This allows easy Mn^{IV} to Mn^{III} reduction and O—O bond formation without crossing over to another spin surface [26,30,32].

The second principal criterion in determining the structures of the proposed intermediates in the S-cycle is that they should each be the lowest energy structure for the given electronic and protonation state of the S-state in question. As the O—O formation step from the S_4 structure was regarded by Siegbahn and co-workers as the most extensively and reliably studied step, the strategy for reaching the other S-state

intermediates involved sequentially and alternately adding electrons and protons to the most favourable S_4 structure as determined in [25] until the S_0 state was reached. For each electron or proton addition step, all possible sites for reduction or protonation were tested in the search for the lowest energy structure (a detailed account of this procedure can be found in [26]). From these, energy level diagrams for the entire catalytic cycle could be constructed, and the plausibility and possible errors in the model could be checked by examining the relative energies of the different intermediates. Over the years, a number of versions of the cycle have been published [26,28,30–33]. Each time refinements were made to address a previous issue in the energetics of the overall scheme, most commonly that of unreasonable/unexpected barrier heights and relative energies of S-state intermediates.

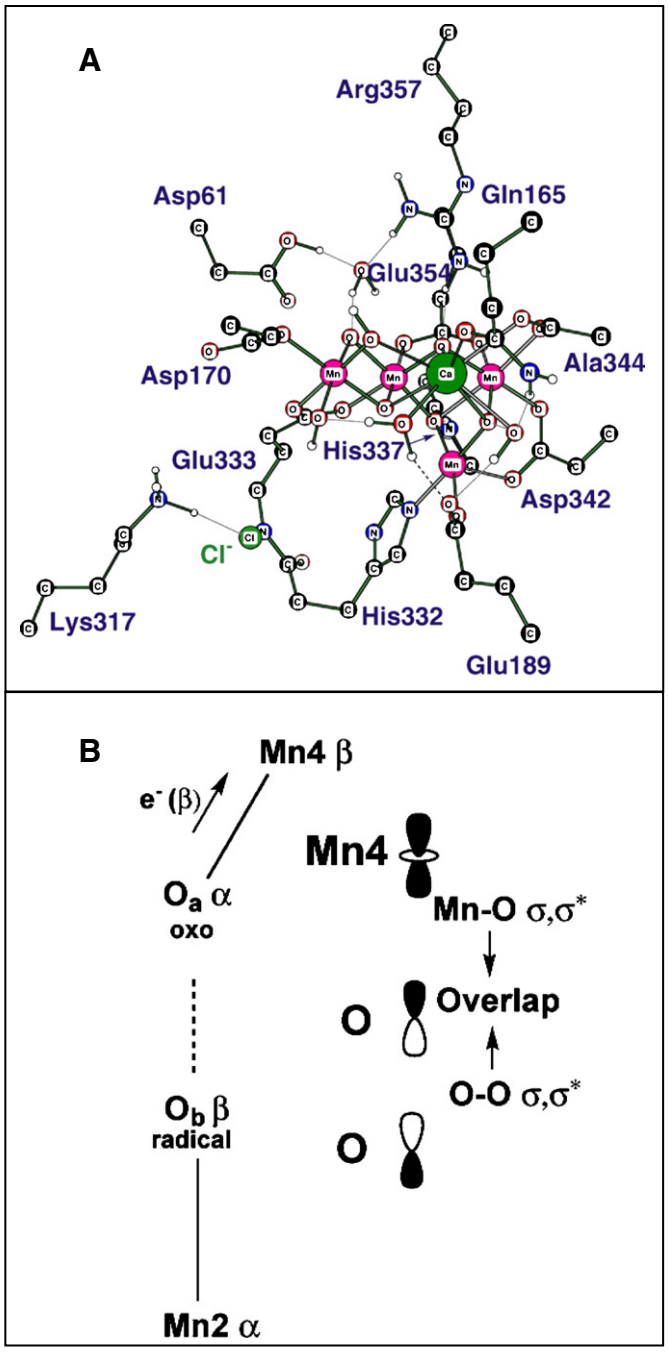

Fig. 1. The cluster model approach used by Siegbahn and co-workers for the study of the water oxidation mechanism. (A) The largest cluster model of the OEC used in the latest DFT cluster model calculations. (Reprinted from Blomberg and Siegbahn [32], with permission from Elsevier.) (B) The Mn^{IV}–$O^{\bullet}$ mechanism for O—O bond formation proposed by Siegbahn and co-workers, including an illustration of the alternating spin alignment for the Mn and O atoms involved. (Reprinted in part with permission from Siegbahn [30]. Copyright 2009 American Chemical Society.)

2.1.2. The S-state cycle—cluster model DFT

The most recent scheme and energy diagram for the catalytic cycle proposed by Siegbahn and co-workers are shown in Fig. 2[30]. The site of oxidation during the $S_1 \rightarrow S_2$ transition is Mn1, with little associated structural change, in agreement with EXAFS data [15,34]. The finding of three short (2.7–2.8) and one long (3.1 Å) Mn–Mn distances in these states is notably more in line with Berkeley EXAFS interpretation [16]. During the $S_2 \rightarrow S_3$ transition, significant structural rearrangement was found, again in overall agreement with the much-debated EXAFS data [13,17]. However, rather than attributing this rearrangement to bond shortening resulting from a Mn-centred oxidation accompanied by the change from a mono-μ-oxo bridge to a di-μ-bridge between two Mn ions (Berlin interpretation [34]), or the lengthening of a di-μ-oxo bridge due to ligand oxidation giving, for instance, a μ–$O^{\bullet}$ species (Berkeley interpretation [15]), Siegbahn has proposed that the binding of a substrate water to Mn2 is the cause of the rearrangement [30]. This binding is accompanied by a deprotonation of the bound water, giving rise to the proton release in this step, and the rearrangement is in part due to steric crowding at the binding site. Interestingly, Mn2 in this model is proposed to be a five-coordinate Mn^{III} ion. Substrate water binding to the open sixth coordination site and subsequent Mn oxidation during the $S_2 \rightarrow S_3$ transition gives a six-coordinate Mn^{IV} in the S_3 state. This is in agreement with the Berlin interpretation of the EXAFS data. However, this Mn-centred mechanism for $S_2 \rightarrow S_3$ transition leads nevertheless to a radical mechanism for O—O bond formation, and the site of the final oxidation of the deprotonated substrate water in the $S_3 \rightarrow S_4$ step. This gives the required Mn^{IV}–$O^{\bullet}$ species for nucleophilic attack by a μ-O-bridge (Fig. 2A). It can thus be seen that the Siegbahn proposal has features that agree with the interpretations of EXAFS data from both the Berlin and Berkeley groups. In fact, the S_3^{-1} ("normal" S_3, Mn^{IV}-OH) and S_3^{-2} (deprotonated S_3, $Mn^{IV}=O$) states were found to be very close in energy (see Fig. 2B), and the spin on the O in the latter case was quite high (+0.40). This led Siegbahn to remark [30] that although formal Mn-centred oxidation is suggested by the mechanism, apparent ligand-centred oxidation character due to the high spin on oxygen could perhaps be observed depending on the experimental conditions. This is an interesting proposal that may help to reconcile the opposing EXAFS interpretations.

Finally, a significant improvement of the latest Siegbahn proposal of the catalytic cycle compared to previous ones is that a O—O bond formation barrier of 10.7 kcal/mol was found (in the absence of a membrane gradient). This is an important result, as it is consistent with the experimentally observed millisecond time scale for O_2 release. In the presence of a membrane gradient, however, the barrier was still too high at 18.2 kcal/mol. This was regarded as possibly stemming from an error in the energy for the S_2 state, either due to the DFT method used (expected error around 3–5 kcal/mol [35]) or potentially an underlying problem with the cluster model.

2.2. QM/MM model

2.2.1. Methodology—QM/MM

The approach taken by Batista and co-workers [36–44] to arrive at their mechanistic proposal for the S-cycle differs from that of Siegbahn and co-workers in two main aspects. Firstly, a hybrid quantum mechanics/molecular mechanics (QM/MM) approach was taken. Secondly, the methodology by which the structures of the S-state intermediates were determined was more reliant on a S_1-state starting structure based on X-ray crystallography data, combined with adjustments to fit other experimental spectroscopic data. This is in contrast to Siegbahn's approach that emphasised energy considerations.

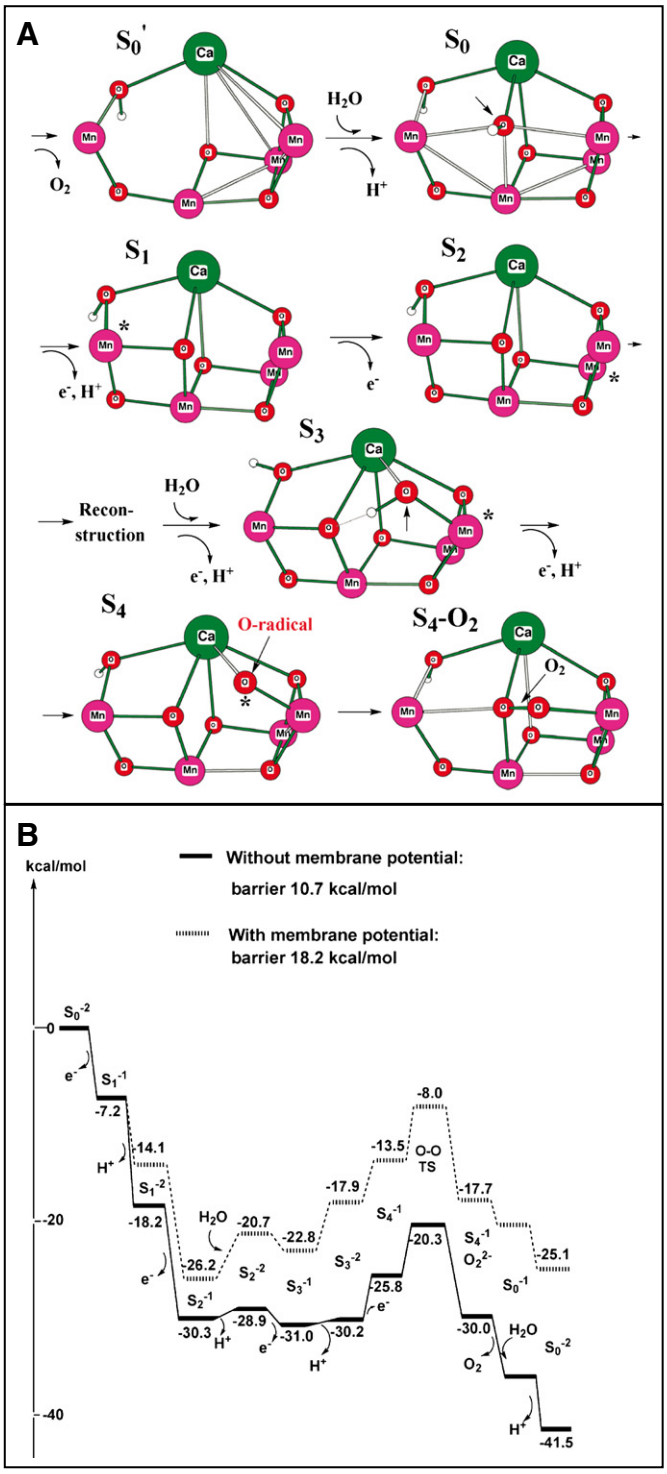

Fig. 2. The mechanism of the S-cycle proposed by Siegbahn and co-workers. (A) The structural and (B) energetics schemes of the transitions between the S-state intermediates. (Reprinted in part with permission from Siegbahn [30]. Copyright 2009 American Chemical Society.)

As alluded to in the discussions above, QM treatments of a system can potentially give high-quality data on mechanistic details including bond formation/breakage and structural rearrangements, but is computationally expensive and restricted to smaller systems. By contrast, MM makes use of forcefields, where molecular parameters such as optimal bond lengths, bond angles, and electrostatic interactions have been parameterised for specific types of atoms, bonding combinations, etc. From this, energies can be calculated for systems in a particular geometry, allowing structural optimisation through searching for energy minima (which may be local or global). Only classical Newtonian mechanics and electrostatics are involved, significantly reducing the computational time required. This allows for the study of much larger systems (10^4–10^6 atoms) than QM methods. However, the results obtained are highly dependent on the applicability of the forcefield for the particular system under study, and MM is by its very nature unable to deal with chemical reaction.

In hybrid QM/MM, the two methodologies are combined. In the so-called ONIOM implementation of QM/MM [45] favoured by Batista and co-workers, the core area of interest where detailed mechanistic information is required (such as the active site of an enzyme) is treated at a QM level of theory (e.g., DFT or HF methods). The effects of regions further away from this core (the protein scaffold beyond the first ligand sphere, for instance) are treated with the less computationally demanding MM. The interaction between the QM and MM layers is also accounted for during the calculations (in practice, even more layers can be defined as required, each treated with a different level of theory; see [45,46]). In this way, proportionally more computational resources are focused on studying the core region of interest, whilst including the effects of the outer regions in a less rigorous, but also less computationally expensive manner.

In the QM/MM calculations carried out by Batista and co-workers, the QM region was treated by DFT, and included the $CaMn_4$ cluster, six ligands as given by the London crystal structure, as well as water and hydroxo ligands and chloride (Fig. 3A). The MM region then extended to a 15 Å radius out from the $CaMn_4$ cluster, together with a harmonically restrained buffer region 15–20 Å from the cluster. A link hydrogen atom scheme was used to define the boundary between the QM and MM layers, and electronic embedding was used to account for interactions between the layers [46]. Thus, a truncated PSII centred on the OEC was simulated, with a total of 1987 PSII atoms being included.

In contrast to the major emphasis on energy as the criteria for constructing a mechanistic proposal of the S-cycle, the work of Batista and co-workers has given more weight to the available structural and spectroscopic data during their structural optimisation procedure. Also, whereas Siegbahn and co-workers first focused on the S_4-state as well as the mechanism and energetics of the O—O bond formation step, the starting point in the Batista studies was the determination of the structure of the dark stable S_1-state [36]. Starting from the OEC and surrounding environment from the London crystal structure, the dark stable S_1-state was first derived from QM/MM structural refinements of the $CaMn_4$ cluster and its associated ligands after hydration of the system with water by "soaking," as well as the inclusion of a Cl^- ion. Two models with comparable energies were then chosen for continued study to obtain the other S-state intermediates, though one of these [model a, with oxidation states ($Mn1^{IV}$, $Mn2^{IV}$, $Mn3^{III}$, $Mn4^{III}$)] formed the basis of the proposed catalytic cycle [42]. The structures of the remaining S states were obtained by sequential oxidation and deprotonation beginning from the S_1-structure, with geometry optimisation being performed at each S-state. Various initial spin states and spin-coupling schemes were also tested by Batista and co-workers using DFT calculations, and the results assessed on both the total energy of the system and comparison to structural and magnetic data in order to select the intermediates in their final catalytic cycle proposal [36,40]. This is shown in Fig. 3B [36,40]. Note that both the electron and (where applicable) the proton(s) associated with each S-state transition were removed before each structural optimisation, giving the "classical" S states S_0–S_4. This is in contrast to the calculations by Siegbahn and co-workers where each individual electron or proton removal step was studied (Fig. 2).

2.2.2. The S-state cycle—QM/MM

The Batista mechanism (Fig. 3B) shares some common features with the Siegbahn proposal above. There is an absence of structural change

during the $S_1 \rightarrow S_2$ transition, and the $S_2 \rightarrow S_3$ transition is proposed to be a Mn-centred oxidation. The "dangler" Mn (Mn4) also undergoes oxidation during the S-cycle, in contrast to a FT-IR study that proposed otherwise [47]. Importantly, the mechanism for O—O bond formation is also nucleophilic attack on a Mn^{IV}–$O^{\bullet}$ species formed during the $S_3 \rightarrow S_4$ transition, rather than a $Mn^{V}=O$ oxo species as had previously been proposed [48,49]. Several differences between the mechanistic proposals can also be found. The site of Mn oxidation during $S_2 \rightarrow S_3$ is Mn4 and the result is a di-μ-oxo bridge formation between Mn3 and Mn4. This is in agreement with the Berlin EXAFS interpretation. Both substrate water molecules were already bound by the S_1 state, unlike a later binding during $S_2 \rightarrow S_3$ for the Siegbahn model. In the Batista mechanism, an initial choice was made that the two substrate water molecules were those that were found to be bound to Ca and Mn4 after initial soaking of the system, in accordance with some previous literature proposals [48–50]. The site of O—O bond formation is at these two ions, where the nucleophile attacking $Mn4^{IV}$–$O^{\bullet}$ is the Ca-bound water, rather than a μ-O-bridge oxygen. It was also suggested that the CP43-R357 residue had a role in deprotonation acting as a redox-coupled base as had previously been proposed [50,51], with its pK_a presumably affected by the OEC in order for it do so [40,43].

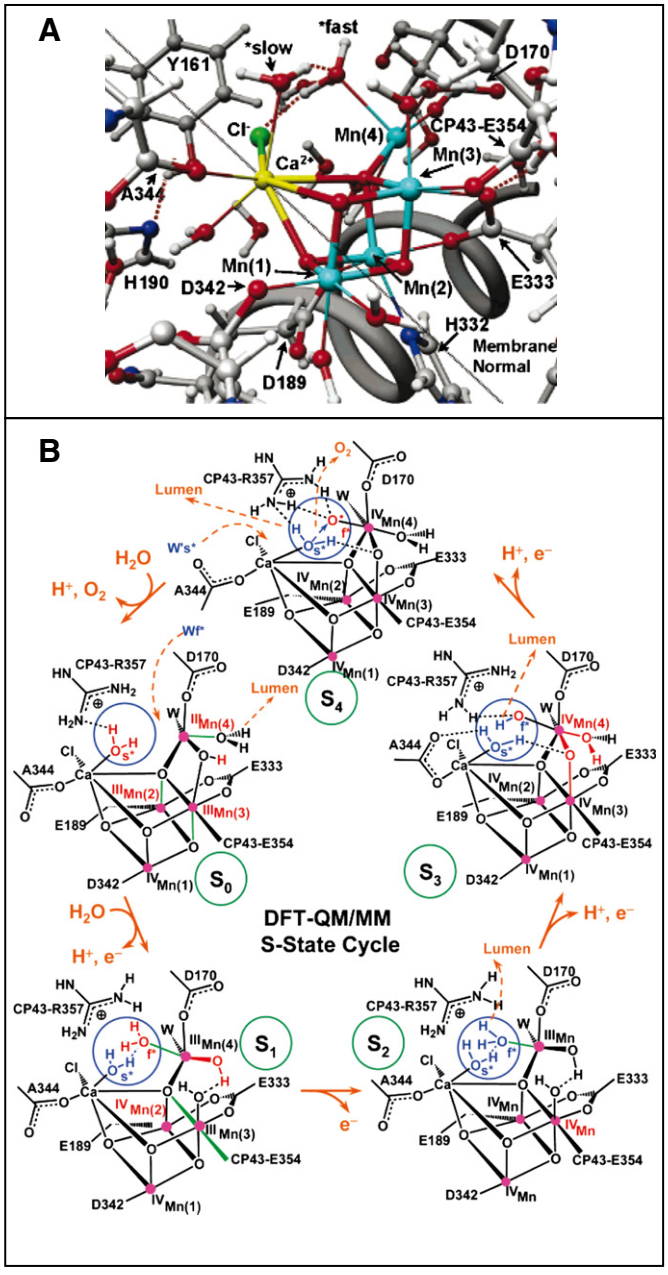

Fig. 3. The QM/MM approach used by Batista and co-workers for the study of the water oxidation mechanism. (A) The energy-minimised starting S_1-state structure as determined by QM/MM calculations. This view focuses on the QM core region of the calculated system. (Reprinted in part with permission from [36]. Copyright 2006 American Chemical Society.) (B) The proposed catalytic mechanism for water oxidation as calculated using QM/MM. Red: changes caused by the immediately preceding S-state transition; blue: substrate water molecules; dashed arrows: changes during the following S-state transition. (Reprinted with permission from Sproviero et al. [40]. Copyright 2008 American Chemical Society.)

To compare the proposed S-state intermediates with the available experimental EXAFS data [14,16], Batista and co-workers calculated theoretical EXAFS spectra [40]. The comparisons of the experimental isotropic EXAFS spectra with those calculated from both the London crystal structure and QM/MM models are shown in Fig. 4A and B. The X-ray model's simulated spectrum deviates substantially from the experimental data (Fig. 4A, upper), while the spectra calculated from the QM/MM models show reasonable qualitative agreement (Fig. 4A, lower, and B). For the structure of the S_1-state, for which experimental polarised EXAFS data were also available, the corresponding calculated polarised spectra based on the QM/MM model (a) could also be compared with experimental data [42]. As Fig. 4C (upper row) shows, there was again good qualitative agreement between the experimental and calculated results, with some clear differences. However, Batista and co-workers found that by using an iterative refinement procedure, the calculated S_1 structure could be adjusted to minimise the deviations between the calculated and experimental EXAFS spectra, finally giving essentially quantitative agreement between the two [42] (Fig. 4C). Interestingly, this refined QM/MM (R-QM/MM) model showed only minor structural differences from the original $CaMn_4$ structure in the London crystal structure (Fig. 4C, lower row).

The energy profiles of the minimum energy paths (MEP) for the gradual detachment of (substrate) water from the Ca^{2+} and $Mn4^{III}$ in the S_1 and S_2 states have also been calculated [44]. The QM/MM calculations found that while it was energetically more demanding in both S states to remove the water molecule bound to Ca^{2+}, the water binding to Ca^{2+} was weakened upon $S_1 \rightarrow S_2$ transition, whereas the reverse was true for the water bound to $Mn4^{III}$. The basis of this was found to be a charge redistribution during the transition that decreased the partial (ESP) charge on Ca^{2+}, whilst increasing the partial charge on $Mn4^{III}$, despite a lack of any formal change in oxidation state in these ions. This was in good agreement with experimental water exchange rates [52], which showed that two water exchange sites exist on the $CaMn_4$ cluster, with one exhibiting faster exchange rates than the other. Furthermore, upon the $S_1 \rightarrow S_2$ transition, the rate constant of the slow exchange site increase, whereas the reverse is true for the fast exchange site. This agrees with the assignment of a fast exchange substrate water site on Ca, and a slow exchange site on Mn4 in the Batista mechanistic proposal (Fig. 3B).

2.3. Comparison of the approaches

From the overviews above, it can be seen that the Siegbahn and Batista groups have taken very different methodological approaches. Siegbahn and co-workers have put heavy emphasis on the energetics of the bond formation steps, the energies of the proposed intermediates, the barriers involved in each individual transition, as well as the plausibility of the overall cycle from an energetics point of view. The starting points of these investigations were relatively model-independent with respect to the sites of oxidation, deprotonation and substrate water binding, though still informed by the structural motifs possible for the $CaMn_4$ cluster. The systematic exploration of the vast number of possible geometric and electronic structures is impressive. While there is not the same extensive direct comparison of calculated spectral data with experimental data as was done in the Batista studies, there are features within the proposed mechanism that correlate with

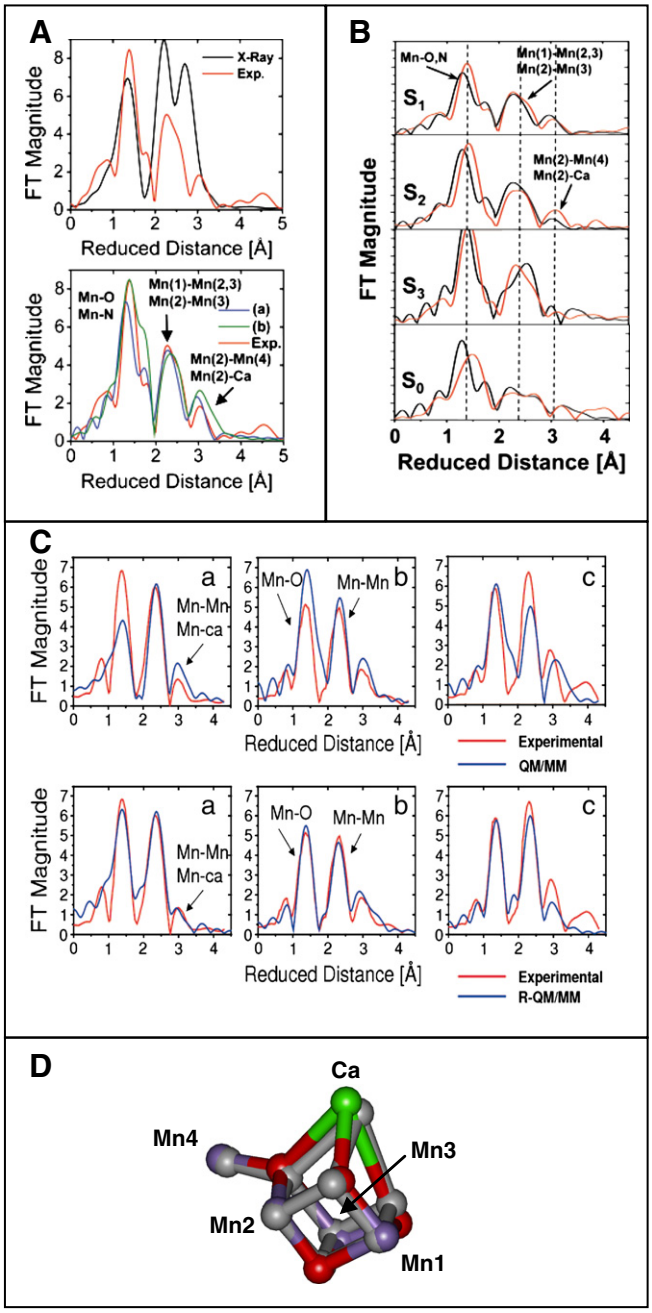

Fig. 4. Comparisons of experimental and simulated EXAFS spectra as calculated on the basis of various models of the OEC. (A) Comparisons of the experimental isotropic EXAFS spectrum of the OEC in the S_1 state with the corresponding simulated spectra calculated on the basis of the London (PDB ID: 1S5L) crystal structure (upper) and the models (a) and (b) of the QM/MM-derived structures (lower). (B) Comparisons of experimental isotropic EXAFS spectra in various S states with the corresponding simulated spectra calculated on the basis of QM/MM model (a). (C) Comparisons of experimental polarised EXAFS spectra in the S_1-state with the corresponding simulated spectra calculated on the basis of the QM/MM model (a) before (upper row) and after (lower row) performing the iterative refinement procedure. Crystallographic axes a, b, c as defined in [16]. (D) Comparison of the position of atoms in the $CaMn_4$ cluster from the London crystal structure (grey) and the R-QM/MM model (coloured; Mn: purple, O: red, Ca: green). Cartesian coordinates for the R-QM/MM model were taken from [42]. (Panels A and B: Reprinted with permission from Sproviero et al. [40]. Copyright 2008 American Chemical Society. Panel C: Reprinted with permission from Sproviero et al. [42]. Copyright 2008 American Chemical Society.)

spectroscopic data and the X-ray electron density maps for the $CaMn_4$ cluster [26,32]. The very detailed and careful consideration and incorporation mechanistic and energetics arguments are compelling. However, as Orio et al. [53] have remarked, computed energies cannot on their own validate a reaction mechanism based on DFT calculations, and more incorporation and direct comparison with experimental data would nevertheless be desirable.

The work by the Batista group has been more reliant on experimental data, both in terms of the starting structure as well as the mechanism and site for O—O formation. The comparisons with isotropic and polarised EXAFS data have provided support for their S-state intermediate structures. Reference to experimental data is clearly valuable and indeed desirable for computational studies. However, their approach was arguably more dependent upon the initial structural model of the S_1-state cluster for the exploration of the possible catalytic cycle. As such, the uncertainties associated with the chosen starting $CaMn_4$ structure and ligand motifs (mostly monodentate), based as they were on the London crystal structure, may have led to an undesirable biasing of the resulting mechanism, perhaps trapping the trajectory within local minima. The O—O bond formation mechanism and substrate binding sites that were chosen from the outset [40] could also contribute to this. This issue is particularly important where a complex reaction landscape is expected of a system such as the OEC, with a wide range of mechanistic possibilities. Clearly, the methodology employed by Siegbahn is not immune to this potential problem either, as some starting structure and mechanism must be chosen. However, the detailed surveys of the energetics and possible alternatives for the starting (S_4) structure, the individual steps of S-state transition throughout the catalytic cycle, as well as for the O—O bond formation step arguably mitigate the situation. Also, the less model-dependent approach leaves more room for adjusting the proposed mechanism to allow for more favourable reaction pathways. This was demonstrated in the change of the S_2-state substrate water binding site and location of the Mn^{IV}–$O^{\bullet}$ species from Mn4 in some earlier proposals [25,26] to Mn2 in the latest scheme [30]. The nucleophilic species attacking Mn^{IV}–$O^{\bullet}$ was also changed from an external water [20] (the same mechanism as in the Batista studies [36,40,50]) to a μ-oxo bridge oxygen [25,30]. In both cases, lower and more reasonable energy barriers were obtained for the reactive steps as a result.

A criticism of the energy-based selection of S-state intermediates favoured by Siegbahn and co-workers has been the margin of error associated with DFT energy calculations on open-shell transition metal complexes using the B3LYP (hybrid) functional. In a benchmarking study [37], Batista and co-workers showed that for at least one multinuclear Mn complex, an incorrect lowest energy spin state was predicted by B3LYP. Large errors of 21–41 kcal/mol were found. It was argued that while the B3LYP functional (used by both the Batista and Siegbahn groups) gives very accurate results for geometric and magnetic properties of complexes, it is too unreliable to allow calculated relative energies to be used for selecting between structural intermediates consisting of open-shell transition metal complexes. (Interestingly, however, the structure of the same multinuclear Mn complex was found to be very insensitive to the spin state, and showed excellent agreement with crystal structure data in all cases, despite the differences in calculated energies.) This is a known drawback of the B3LYP functional [35,53,54]. Siegbahn has argued [35], by contrast, that the large errors found in [37] does not apply across the board for all such complexes. Instead, a margin of error of 3–5 kcal/mol was more usual, especially if the extent of exact exchange content in the B3LYP functional is adjust from 20% to 15% for calculations of such open-shell complexes. Siegbahn has also reported that changes in the spin-coupling schemes between Mn ions in their proposed S-state intermediates had very little effect except in the O—O formation step (as outlined above regarding spin alignment) [25]. Indeed, relative energy is one criterion used for deciding between candidate intermediates even in the studies by Batista and co-workers.

It can be noted that in a comparison of the single point energies of S_1-state models derived from the cluster model and QM/MM calculations, Siegbahn [29] reported that the QM/MM model was over 70 kcal/mol higher in energy than the cluster model S_1 state.

Even assuming that the cluster does not have to exist in its lowest energy conformation in PSII, the energy barrier for decay to a lower energy structures was found to be too low for the QM/MM structure to be stable. A similar comparison was made with 10 proposed S_2 state structures that were based on structure motifs from polarised EXAFS combined with DFT calculations employing a variety of spin-coupling parameters and spin models [55]. It was shown that the cluster model S_1-state was around 34–63 kcal/mol lower in energy than these alternatives [29]. However, as Batista and co-workers have pointed out [44], even 3–5 kcal/mol margin of error would be too high to calculate the activation barrier for water exchange (2–3 kcal/mol). Water exchange was therefore studied using the energy profile of the MEP for stretching the water–(Mn, Ca) bond instead [44].

The fits of the calculated polarised EXAFS spectra derived from the R-QM/MM structures by Batista and co-workers to the experimental EXAFS data were certainly excellent, and gave experimental support for the plausibility of the suggested S_1-state structure. An interesting observation, however, is that only minor adjustments to the unrefined QM/MM model were required to produce the R-QM/MM model that gave the quantitative fits between the calculated and experimental spectra (Fig. 4C). These fits were at least as good as the other four models presented in polarised EXAFS study [16]. Furthermore, this R-QM/MM model deviated only slightly from the original London crystal structure (Fig. 4D). Now the cuboid $CaMn_4$ cluster from the London structure (and by extension the R-QM/MM structure) is substantially different from the four EXAFS models [16]. In addition, the geometry of the cluster in the London structure is likely to have been altered due to radiation damage [1]. So the fact that quantitative fits could be achieved for each of the R-QM/MM model as well as the other four models in [16] raises the question as to how unique the solutions for the fitting of the calculated polarised EXAFS are with respect to the structure of the $CaMn_4$ cluster, and therefore how diagnostic such fits really are for determining the validity of a proposed structural model. It should be kept in mind that while a plausible structural model for the cluster must give good fits to the polarised EXAFS data, good fits to EXAFS data as such are not sufficient proof that the suggested structure is correct.

3. Channels in PSII

Another aspect of the PSII structure that has recently received attention in the literature is the possible existence of channels in the PSII protein complex [56–58]. As the $CaMn_4$ cluster is buried within the D1 protein subunit, it was proposed even prior to the availability of the crystal structures that specific channels may exist in the protein matrix to allow substrate water to access the catalytic site, and for the protons and O_2 that are produced to leave ([59,60]). Channels for water have been suggested to ensure optimal binding and orientation to the cluster, and to avoid side-reactions associated with an excessive amount of water, whereas H^+ pathways are need to transport H^+ efficiently via the Grotthuss mechanism (see below). Efficient removal of O_2 through channels has been suggested to prevent singlet O_2 formation due to O_2 reacting with P_{680} in the triplet state that can be formed through charge recombination (reviewed in [57,61]). Analogous channels have also been found to exist in a variety of other protein complexes, such as acetylcholinesterase, cytochrome *c* oxidase and aquaporin (for an overview of studies of channels in other enzyme systems and more detailed discussions of computational simulation strategies relevant to different kind of channels in those systems, see [61]).

A number of computational efforts have been made to identify channels in PSII by looking for continuous/contiguous spaces within the protein complex that would be able to accommodate a water-/O_2-sized probe in the available crystal structures [56–58]. As H^+ transfers would involve water molecules, this also gave clues to such pathways' possible locations. Slightly different methodologies were employed in these studies. In Ho and Styring [57], all possible solvent accessible regions around the $CaMn_4$ were calculated from the crystal structure (PDB ID: 2AXT, [3]), and the full solvent contact surface was then examined in detail to locate the channels. By contrast, in both Murray and Barber [56] and Gabdulkhakov et al. [58], the software CAVER[62] was used to conduct an automated search of the PSII crystal structures (PDB ID: 1S5L [2] and 3BZ1 [4], respectively) for trajectories of channels leading from the position of the $CaMn_4$ to the lumen, giving profiles of the paths identified and the diameter of the channel along these paths. A comparison of the locations and orientations of various channels identified in the different studies is summarised in Fig. 5 and Table 1.

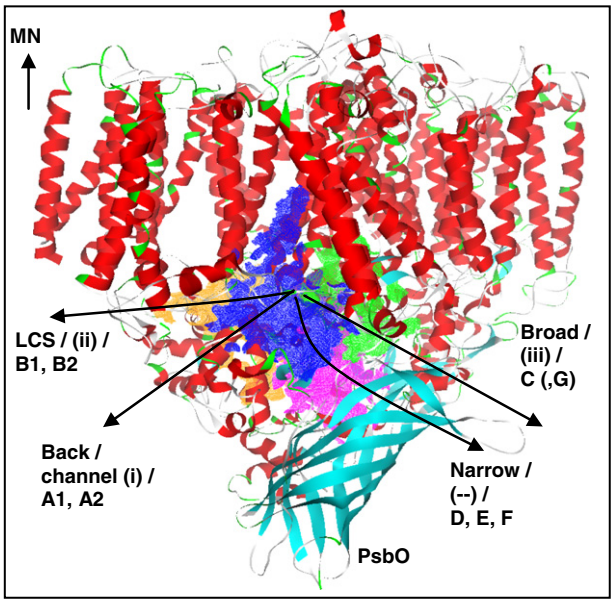

Fig. 5. The positions and orientations of the various channel proposals for PSII [57]. The names of the channels are taken from the studies in the following order: Ho and Styring [57]/Murray and Barber [56]/Gabdulkhakov et al. [58]. See accompanying text and Table 1 for more details. MN: membrane normal; LCS: large channel system.

3.1. Water channels

Three sets of channels were found to connect the $CaMn_4$ cluster to the lumen were identified by Ho and Styring [57], and they were named the "back channel," "narrow and broad channels" and the "large channel system" (Fig. 6). Of these, the back channel (Fig. 6A) was proposed to function as a water channel, though perhaps not exclusively, given that the large channel system (Fig. 6C) is also likely to be filled with water. An interesting feature of the back channel is that, while it is in contact with Ca^{2+}, it would be necessary for water molecules to cross a gap formed by the residues D1-Y161, -H190, -E189, -P186, -Q165 and the Ca^{2+} in order to reach the Mn ions via the distal section of the broad channel (Fig. 6D). These same residues have been proposed to be of special importance in water oxidation [41,63,64], and it was suggested that this gap could serve as a control gate for regulating the extent of substrate water access to the $CaMn_4$ cluster through transient changes in the diameter of the opening under dynamic conditions. This was in line with various suggestions in the literature that some control mechanism may exist to optimise and regulate the access of water to the $CaMn_4$ cluster, including a possible "gatekeeper" function for Ca^{2+}[57] (the gap no longer exists when the Ca^{2+} is removed from the crystal structure and the solvent accessibility analysis is repeated).

Murray and Barber [56] also identified three main channels, named channels (i), (ii) and (iii). Of these, channel (i) corresponds to the back channel in Ho and Styring, with a very high degree of agreement between the two studies. However, channel (i) was assigned as an O_2 exit, with the authors preferring instead channels (ii) and/or (iii) for water entry and proton exit (Table 1 and text below). The back

Table 1
Residues near the $CaMn_4$ cluster involved with the channels identified in the PSII crystal structure.

	Name	Transport of		Name	Transport of		Name	Transport of		Name	Transport of	
Ho and Styring (2008)	Back	Water		Narrow	H^+		Broad	H^+		Large	O_2	
Murray and Barber (2007)	(i)	O_2		–	–		(iii)	Water/H^+		(ii)	Water/H^+	
Gabdulkhakov et al. (2009)	A1, A2	Water		D, E, F	H^+		C (, G)	H^+		B1, B2	O_2	
Residues within 15 Å of the $CaMn_4$ cluster, based on channels in Ho and Styring (2008)	D1	-Asn	87	D1	-Asp	61	D1	-Ile	60	D1	-Glu	189
		-Ala	88		-Gly	62		-Asp	61		-Glu	329
		-Ile	89		-Ile	63		-Ile	63		-His	332
		-Gly	90		-Asn	87		-Glu	65		-Pro	340
		-Leu	91		-Glu	333		-Val	67		-Leu	341
See the original publications for full residue listings.		-Tyr	161		-Ser	169		-Pro	84		-Asp	342
		-Ile	163		-Asn	335		-Tyr	161		-Leu	343
		-Gly	164		-Ala	336		-Ser	169		-Ala	344
		-Gln	165		-Asn	338		-Asp	170	CP47	-Arg	384
		-Gly	166	CP43	-Pro	334		-Gly	171	CP43	-Glu	354
		-Glu	189		-Thr	335		-Met	172		-Met	396
		-His	190		-Leu	337		-Pro	173		-Ala	399
		-Asn	296		-Met	342		-Asn	181		-Leu	401
		-Asn	298		-Gly	353		-Phe	182		-Gly	409
		-Asp	342		-Glu	354		-Val	185		-Val	410
		-Leu	343		-Met	356		-Phe	186		-Thr	412
		-Ala	344		-Arg	357		-Met	331		-Glu	413
	CP43	-Trp	291					-His	332	D2	-Arg	348
		-Phe	292					-Glu	333		-Ala	351
		-Gly	306					-Arg	334		-Leu	352
		-Phe	307				D2	-Glu	312	PsbU	-Tyr	133
		-Ala	309					-Phe	314	PsbV	-Lys	160
		-Met	356					-Lys	317			
		-Arg	357					-Leu	320			
		-Phe	358					-Leu	321			
		-Ala	399									
		-Pro	400									
		-Leu	401									

channel/channel (i) was also identified in Gabdulkhakov et al. [58], named there channels A1/A2, where they were also assigned as water channels. Channels A1 and A2 overlapped to a very high degree, and their bifurcation near the luminal surface stemmed from a slightly different position of a lipid molecule (DGD2, Fig. 6A) in the 2.9 Å-resolution crystal structure (PDB ID: 3BZ1, obtained from reprocessing of the X-ray diffraction data set used to produce the PDB ID: 2AXT structure). Additionally, channels B1/B2, C, D, E, F and G were also reported in Gabdulkhakov et al. and assigned to O_2 and proton removal functions (Table 1). These are considered further below.

A significant limitation of these studies based on the crystal structures of PSII is that only a particular static conformation of the protein complex is considered. As discussed in Ho [61], there is significant movement or "breathing" in the protein structure under dynamic physiological conditions, such that important information about dynamic processes may be missed by considering the static structure alone. To overcome this limitation, Vassiliev et al. [65] performed a 10-ns molecular dynamics (MD) simulation of a PSII core complex in the presence of explicit solvent water molecules in order to identify channels from a dynamic view point. In MD simulations, classical Newtonian laws of motion are used to simulate the thermal motions of a system over time [18]. As for MM, forcefields are used for the calculations.

To analyse the resulting MD data, Vassiliev et al. used a diffusion tensor tracking method to generate fibre tracks or "streamlines" to analyse the movement of water molecules, thus revealing the paths most likely to be heavily trafficked by water molecules. This was a novel implementation of an analysis and visualisation method until now mainly restricted to medical imaging [66]. A large number of water paths were found from this MD simulation. Not only were water streams found in all of the channel systems described in [57], the MD simulations also revealed a number of new tracks and exit points not found in earlier analyses. For example, the blockage at the end of the broad channel could be circumvented by a water flow around this point, streamlines were found to connect the narrow channel to both the large channel system and the broad channel distal from the $CaMn_4$ cluster, and a group of previously unknown water tracks were found to join up with the large channel system. On the other hand, at certain points of some water-filled channels (e.g., back channel), there were discontinuities in the water streams, suggesting that some other factors such as hydrophobicity affected or disrupted potential water flow. Vassiliev et al. found that water could flow from the lumen to the $CaMn_4$ via numerous paths, with the large channel system supplying the most. This is reasonable given its size and numerous exits, and as pointed out in earlier studies [56–58], the suggested channels functions may not be exclusive. Overall, the distribution, exact trajectories and the dynamic behaviour of the water molecules and protein were much more complex than could be predicted from the static structures alone.

Two further particular interesting observations were found in this MD study by Vassiliev et al. [65]. Firstly, transient opening and closing of channels were observed. Given the multitude of paths available for water movement between the lumen and the $CaMn_4$ cluster, Vassiliev et al. suggested that the availability of substrate water is unlikely to be a problem in PSII. Nevertheless, at the $CaMn_4$ cluster, the dynamic movement of a set of residues led to the intermittent opening up of water access paths to the $CaMn_4$ via the back channel/channel (i)/channel A1-A2. This occurred near the water control gate proposed in Ho and Styring [57], with the residues observed to be involved showing some though not identical correspondence between the two studies. In addition, the MD simulation revealed that there was also transient opening and closing of a number exits in the large channel system. These exits could intermittently disrupt water exit/entry as indicated by the water streams. These observations therefore support the idea that some regulatory mechanism could exist to control water flow or access to the $CaMn_4$ cluster.

Secondly, Vassiliev et al. [65] also performed a MD simulation on a PSII core complex where the $CaMn_4$ cluster had been removed in silico.

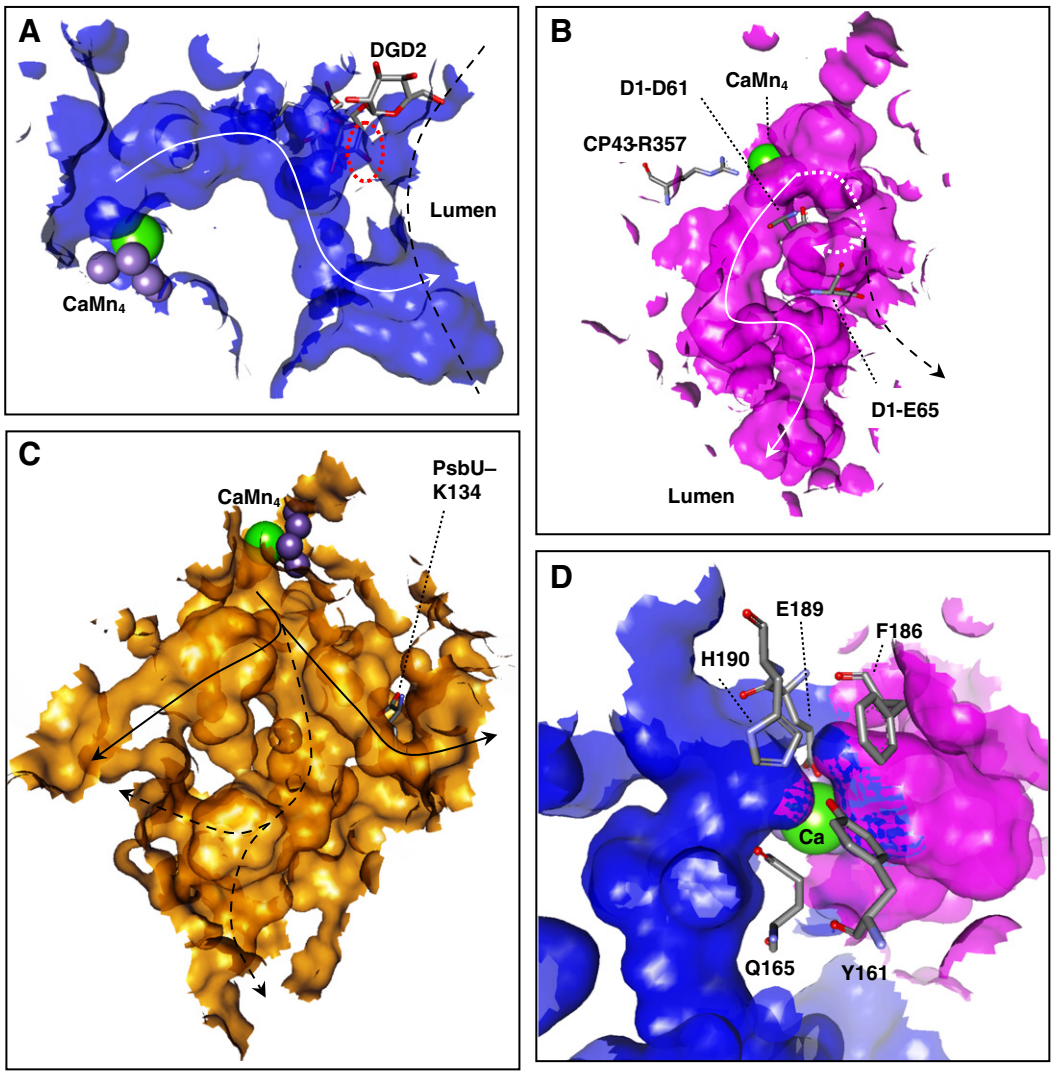

Fig. 6. The water, H^+ and O_2 channels proposed in Ho and Styring [57]. (A) The back channel. A slightly different position of the DGD lipid in the 2.9 Å crystal structure [4] leads to the bottleneck (dotted oval) becoming wider (channel A1 in [58]). (B) The narrow (solid arrow) and broad (dotted arrow) channels. The continuation of the broad channel past the blockage (see text) is marked with a dashed black arrow. (C) The large channel system, with the various branches marked with arrows. (D) The gap between the back and broad channels, located at the Ca of the $CaMn_4$ cluster, which may function as a control gate for water access.

It was found that this led to a very interesting change in the protein structure, such that the back channel became straighter and wider compared to that found in the native PSII. The diameter of the channel became suitable for the passage of ions such as Cl^-, Ca^{2+} and Mn^{2+}, and it was suggested that this change in protein structure upon Mn-depletion could reflect a pathway for the entry of these ions during $CaMn_4$ cluster assembly. This is a particularly interesting proposal that further demonstrates the potential of MD simulations to give insight into processes at a molecular level.

3.2. Oxygen channels

In each of the studies locating channels on the basis of the PSII crystal structures, possible O_2 channels were proposed (Table 1, Fig. 6C). In Murray and Barber [56] channel (i) was assigned such a function. This channel corresponds to the back channel in Ho and Styring [57], where this channel was instead assigned the function of water transport. By contrast, the large channel system was proposed in Ho and Styring as being preferable for O_2 exit. Of the channels identified in that study, this channel system was the largest by volume, consisting of three main branches leading to four exits (Fig. 6C). Since O_2 should be removed efficiently to avoid $^1O_2$ formation, this channel system was geometrically speaking a better candidate for O_2 exit. The presence of the non-polar O_2 molecules in a larger, water-rich cavity would also lead to less significant disruption of hydrogen bonding between water molecules compared to O_2 molecules in narrower channels with fewer water molecules present. The branches of this channel system were found to radiate from the $CaMn_4$ cluster and along the surface of the PsbV subunit, akin to ski slopes down a hill. Although suggested as being favourable for O_2 transport, the possibility that the large channel system could provide substrate water access to the $CaMn_4$ cluster was not excluded, since it is also most likely to be filled with water. Indeed, this was observed in the MD simulation study by Vassiliev et al. [65].

Comparing the large channel system in [57] to the other studies, the channel designated channel (ii) in Murray and Barber [56] partially overlapped with the left and right branches as shown in Fig. 6C. The central "trunk" of the system (dashed arrows) was not reported there. The same result was reported in Gabdulkhakov et al. [58], where the left and right branches in Fig. 6C were designated

channels B1 and B2, respectively. Again, the central trunk of the system was not reported. While Murray and Barber assigned channel (ii) to water and proton transport, Gabdulkhakov et al. were in agreement with Ho and Styring in assigning an O_2 transport function to these channels. Gabdulkhakov et al. also suggested that the residue PsbU-K134 could open or close channel B2 depending on its conformational orientation (Fig. 6C).

To give experimental support for their computational assignment, Gabdulkhakov et al. [58] performed noble gas perfusion experiments to identify how O_2 may be transported away from the site of water oxidation. This was one of three such perfusion studies in recent years [4,58,67]. Although up to 26 binding sites were found in the transmembrane region of each the PSII monomer in these studies, no Xe binding sites were found within the proposed O_2 channels. Kr perfusion by Gabdulkhakov et al. [58] revealed two Kr binding sites, one in each of channels B1 and B2, though otherwise no other binding sites were found within the channels. Gabdulkhakov et al. argued that the Kr perfusion data provides support for their O_2 channel assignments, with a number of Xe sites also forming an additional path for O_2 exit. However, it should be noted that the Xe binding sites proposed to be this O_2 exit pathway are found at the transmembrane interface between two PSII monomers, not within the monomers proper (Fig. 7; see also Table 3 in [58]). As such, the physiological significance of these sites is not entirely clear. Furthermore, care should be taken in interpreting the results of Xe-perfusion studies as indicators of O_2 transport channels. A lack of crystallographically resolvable binding sites should not automatically be equated with a lack of O_2 exit pathways. Considering the underlying basis of the perfusion experiments more carefully, the absence of Xe binding sites can be quite consistent with (though certainly not proof of) efficient removal of O_2 through certain pathways or channels. In the case of channels for O_2 exit in PSII, rapid O_2 exit rather than high affinity binding is desired. A channel system through which Xe (O_2) is able to move efficiently will not necessarily give rise to stable and ordered binding of the gas molecules—this is most likely not even desirable. The resulting disorder in Xe positions would not give resolved electron densities in the diffraction data, and therefore would not be visible. The very ability of Xe to indicate O_2 binding is not necessarily compatible with the aim of identifying channels for O_2 exit in PSII.

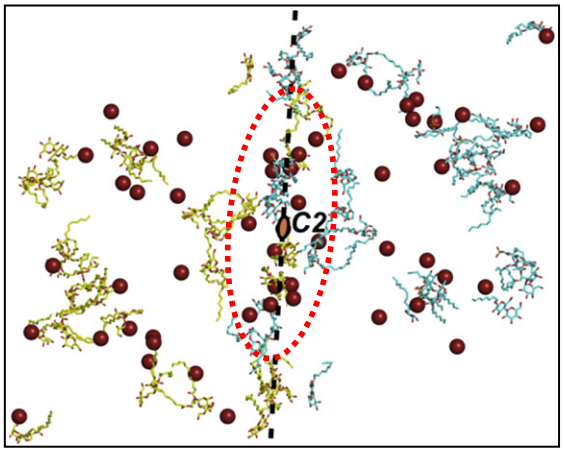

Fig. 7. The position of the Xe sites (red spheres) in the PSII dimer as identified by Xe-perfusion studies in Gabdulkhakov et al. [58] viewed from the lumen along the membrane normal. The monomer–monomer interface is marked with a dashed line. The centre of the pseudo-C2 axis of the dimer is marked with an orange oval. The lipid molecules in each dimer are also shown, yellow for one monomer, and blue for the other monomer. The Xe sites that were proposed to act as an O_2 channel in [58] are marked with a red dotted oval, showing their location at the monomer interface rather than within the monomers themselves. (Reprinted from Gabdulkhakov et al. [58], with permission from Elsevier.)

3.3. Proton pathways

Protons are released in specific S-state transitions during water oxidation, and it has been proposed that such release alternates with electron release in order to achieve "redox-levelling," thereby allowing the same oxidant, $Y_Z^{\bullet}$, to function for all transitions (reviewed in [13]). This is also consistent with the proposed mechanisms as calculated from DFT [32,41]. Any proton exit pathway for PSII would therefore be expected to be efficient so as not to retard the S-state cycle. As "naked" protons do not exist in aqueous environments, their movement through the protein must be conducted via water and/or amino acid side chains. The generally accepted model for this is the Grotthuss mechanism, which has seen much theoretical development since it was first proposed early in the 19th century [68] (for reviews, see [69–71]). Through the interconversion of covalent bonds and hydrogen bonds of water molecules around the hydrated excess proton, the proton is effectively passed through a network of hydrogen-bonded water molecules (often referred to as "proton hopping"). More precisely, there is an interconversion of the hydrated proton across a continuum of two conformational extremes, namely, an Eigen cation $[(H_2O)_3H_3O]^+$ and a Zundel cation $[H_2O\text{-}H^+\text{-}OH_2]$. The proton that exits is not the same as the one that entered in the first place, and in principle, (de-) protonatable amino acid side chains can also participate in the proton transfer.

It is not likely that just any random path in the protein would suffice. Specific and well-tuned proton transfer pathways are known in a number of other biological systems, including cytochrome *c* oxidase and bacteriorhodopsin and carbonic anhydrase (see Ho [61] and Swanson et al. [70] for reviews).

Apart from efficiency, there is also the question of directionality. The synthesis of ATP by ATP synthase at the end of the photosynthetic electron transport chain is driven by the proton gradient that is established across the thylakoid membrane during the light-driven reactions. The released protons must be moved against the proton gradient in order to establish and maintain it. As a result, some local tuning of electrostatic potentials is likely to be required to ensure directionality of proton transport, and to avoid proton back-flow.

From a direct examination of the amino acid residues around the $CaMn_4$ cluster as revealed in their fully refined 3.5 Å-resolution crystal structure, Barber and co-workers [2,72] proposed that the proton exit channel started at the D1-D61 residue, and proceeded through the D2 subunit and then across the neck region of the extrinsic PsbO protein, involving the residues D1-E54, D2-K317, -E312, PsbO-D158, -D222, -D223, -D224, -H228 and -E229 (PDB ID: 2AXT/3BZ1 numbering). The possibility that this channel could additionally act as a water channel was also raised.

A proton exit pathway and a water entry channel were also proposed by Ishikita et al. [73] on the basis of calculated S-state dependent changes in the pK_a of residues near the $CaMn_4$ cluster. A monotonic increase in pK_a of these residues going away from the $CaMn_4$ cluster was found. A number of residues (D1-D61, -D59, D2-K317 and CP43-R357) underwent particularly large changes during the $S_4 \rightarrow S_0$ transition. Although the absolute magnitudes of change in pK_a values may not necessarily be realistic, since the Mn ions accumulated very high charges (+4 between the S_0 and S_4 states) without explicit consideration of charge compensation by proton release, the observed trends in S-state dependent changes may nevertheless give valuable clues as to which residues may be involved in the proton exit pathway.

Beyond an examination of the identity of the residues around the $CaMn_4$ cluster, the three channel studies [56–58] have yielded similar, but not identical proposals for the proton channels (Table 1, Fig. 5).

The structural search using CAVER by Murray and Barber [56] assigned a channel designated channel (iii) as the proton channel on the basis of its narrowness, hydrophilicity and correspondences to the residues in the proposed proton channel in Ferreira et al. [2]. Starting from D1-D61, D2-K317, D1-D59, D2-E312 and D1-E65, it passes across

the top of the PsbO barrel (R152, D158, D222, D224, H228, E229) on its way to the lumen. This is essentially in agreement with the earlier proposal by Barber and co-workers (above). In the analysis by Ho and Styring [57], this channel corresponds at the $CaMn_4$ to the "broad channel," which is connected to the "narrow channel." These channels make contact at their proximal ends with the Mn ions (especially Mn4) of the $CaMn_4$ cluster, in the vicinity of the residues D1-D59, -D61, -E65, D2-K317 and CP43-R357. The narrow channel then extends all the way to the lumen, passing through mainly the CP43, PsbO and PsbU subunits, with the exit formed by CP43 and PsbU residues. This narrow/broad channel system was also suggested as serving as a proton exit pathway.

There are two key differences between the narrow/broad channels and channel (iii). Firstly, the narrow channel was not reported in Murray and Barber [56], but the presence of this channel and the movement of water within it have been confirmed in the recent MD simulations [65]. Secondly, whereas channel (iii) and the broad channel coincided near the $CaMn_4$ cluster, the broad channel was found to have a bottleneck at D1-E54, D1-P66, D1-V67 and D2-E312 that was too narrow for passage. Beyond this point, however, an open channel towards the lumen was observed, as in Murray and Barber. It is likely that these differences in results are due to the different simulation methodologies used [57]. Note, however, that whether channel (iii)/broad channel is open is not critical here, given that proton movement does not necessarily require a fully open channel for Grotthuss-type proton transfer, if intervening protonatable amino acids that are able to participate in the transfer are present. Also, as mentioned in section 3.1, Vassiliev et al. [65] found water streamlines that circumvented this apparent blockage.

In both studies, reliance was placed on literature experimental data, suggesting that D1-D61, D1-E65 could be involved in a proton exit pathway [74], as well as on calculated S-state dependent pK_a changes [73]. Murray and Barber pointed out further that a Ca^{2+} binding site in PsbO was located near the exit of channel (iii), and therefore could play an electrostatic role in assisting proton transfer into the lumen. It has also been proposed from structural considerations and QM/MM calculations that the CP43-R357 residue, which is part of the narrow channel [57], is involved in deprotonation steps during the S-cycle [40,50]. Furthermore, both the cluster model DFT and the QM/MM models agree that D61 is a likely starting point of a proton exit pathway. A mechanism for proton translocation from the $CaMn_4$ via a network of hydrogen-bonded water molecules and residues, including D1-D61 and D1-E65, was also proposed in [40].

In the more recent analysis of the of the 2.9 Å crystal structure [4] by Gabdulkhakov et al. [58], again using CAVER, a smaller probe radius criterion than that in Murray and Barber [56] and Ho and Styring [57] was used to identify possible proton channels. All channels that were not wide enough for transport of O_2 or water molecules, but which could accommodate the presence of water molecules, were regarded as possible candidates. Breaks in continuity not longer than about 3.5 Å (maximum distance between heavy atoms in a hydrogen bond) were permitted. This is a reasonable additional test, given the nature of the Grotthuss mechanism. From this analysis, a set of channels named channels C–G were assigned as proton exit pathways. A closer examination of these channels reveals that there is a high degree of overlap between these channels (channels D, E, F share a large number of residues, as do channels C and G), and they are essentially in agreement with the putative proton channels identified in Murray and Barber and/or Ho and Styring (see Table 1), with the exception of the distal section of channel G that leads to a previously unknown exit. Overall, the larger number of pathways identified in [58] appears to be mainly due to the smaller probe radius used, and in allowing reasonable breaks in the channel to account for the mechanism of H^+ transport.

Despite differences in the details, the various proposals for the proton exit pathway are in good general agreement, and it would seem that they do describe the most likely region where the pathway lies. Studies that take protein dynamics (e.g., using MD) and energetics (reviewed in [61,75]) into account will shed further light on this. Indeed, our recent 10-ns MD study of a chain of residues in this very region has shown that there is a hydrogen-bonded chain of residues and water molecules leading from the $CaMn_4$ cluster to the lumen [76]. It was found that there is a "hotspot" network of highly interconnected residues and water molecules around D1-D61 and -E65. Not only were these two residues found to be connected by water bridges almost 100% of the time, in agreement with their proposed role in H^+ transport via the Grotthuss mechanism, it was also found that the stability of this chain was greatly influenced by the balancing of hydrogen bonding interactions with other residues in the channel that would not otherwise be expected to participate in H^+ transport. In particular, the D1-R334 residue was found to be highly water bridged to D1-E65, and parallel MD simulations showed that the mutations to R334V and R334E in silico led to a very significant disruption of this putative H^+ pathway. Substantial changes to the conformations of the residues in the pathway were observed, as well as a lengthening and destabilisation of the connection between D1-D61 and -E65. This is in good agreement with experimental mutagenesis data that has also shown reduced O_2 evolution activity, slowed down flash O_2 release kinetics, and disrupted S-cycle behaviour due to these mutations [77].

4. Other computational studies

In this final section, a short overview of some other selected computational studies related to PSII structure and function will be present.

4.1. Structural effects on electron and energy transfer

In the present review, the focus has been on computational studies that have directly involved the characteristics and dynamics of the PSII structure itself. There is also a large body of literature concerning the calculation and simulation of the excitation dynamics and spectral characteristics of photosynthetic systems. These studies have as their focus the theory and modelling of the physical processes involved in energy and electron transfer processes during light harvesting and charge separation, with the structure of PSII being important mainly for the relative positions and orientations of the pigments and co-factors in question. Readers interested in these studies are referred to a number of recent reviews on the subject [78–83].

One particular study that explicitly considered the effects of PSII structural dynamics on the spectral and energetic characteristics is that by Vasil'ev and Bruce [84]. MD simulation of a PSII core complex revealed how the distance and orientation between pigments and co-factors involved in energy transfer and charge separation vary under dynamic physiological conditions. The influence of this variability on the site energies of the antenna Chl's and their subsequent influence on PSII spectral characteristics as well as energy and electron transfer efficiencies were investigated using QM calculations. Energy transfer in light harvesting was calculated using Förster theory for excitonically coupled systems, and electron transfer rates were derived from the so-called "Dutton's ruler" [85]. It was found that whereas the simulated absorption spectrum of the PSII core complex calculated directly from the position of antenna Chl's from the crystal structure did not match experimental results, calculations based on several snapshots of the MD simulation trajectory led to spectra that agreed well with experiments. The site energies of Chl molecules were found to fluctuate significantly, and the position of Q_B was found to vary between two binding conformations. Furthermore, strong fluctuations were observed in the calculated rates of Pheo to Q_A electron transfer. The fluctuations in Chl site energies and Pheo to Q_A electron transfer rates were found to have a greater impact on photochemical efficiency than the changes in the relative positions and conformations of the antenna Chl's. This study demonstrated how protein dynamics can affect energy and electron transfer rates in PSII, and can be compared with other MD/QM studies that have been performed on the

much better characterised bacteriochlorophyll and light harvesting complex LC2 of bacterial reaction centres [86–88].

4.2. Diffusion of PSII and plastoquinone in thylakoid membranes

After Q_B accepts two electrons from Q_A, the resulting plastoquinol Q_BH_2 leaves the Q_B pocket and diffuses to the Cytb_6f complex. This pocket then needs to be replenished with plastoquinone. Channels lined with hydrophobic lipids that facilitate this have been proposed, based on examination of the crystal structure [4]. It was also proposed that a third plastoquinone, Q_C, located in a nearby binding site, may be involved with this mechanism. But how do the plastoquinone/plastoquinol molecules diffuse through the protein-packed thylakoid membrane, with a density of membrane proteins of ~70% [89]? Furthermore, since repair of damaged PSII complexes takes place in the lamella region of thylakoid membranes in higher plants [90,91], how do they diffuse efficiently enough from grana regions, given that theory would predict only a mean diffusion distance of 10 nm (about half the size of a PSII supercomplex) in 1 min[92]?

By employing percolation theory and Monte-Carlo simulations of random walk diffusion processes, Kirchoff and co-workers examined the diffusion distance of plastoquinone molecules in thylakoids (reviewed in [93]). It was found that [89,94] below a critical density of randomly placed PSII complexes (estimated from the calculations to be around 60–70%), plastoquinone would be able to freely diffuse throughout the membrane. Above this critical density, however, microdomains would form, within which the diffusion of plastoquinone would be restricted. This was particularly interesting in that, at ~70% protein density, a microdomain size of around 20 nm would be obtained, so that not all PSII would theoretically be close enough to a Cytb_6f complex for plastoquinol diffusion to the latter [94].

It would appear that the solution to this problem, and that of efficient PSII complex diffusion, may lie in the formation of PSII supercomplexes, as well as the supramolecular order of PSII complexes in the thylakoid membrane [93]. Again, on the basis of Monte-Carlo simulations and percolation theory, it could be shown that for the same protein density, larger particles such as supercomplexes lead to less diffusion obstacles, and thereby more efficient diffusion for both small molecules such as plastoquinone/plastoquinol [94], as well as the complexes themselves [92]. The parallel alignment of PSII complexes that are sometimes observed in electron microscopy and AFM studies [95] may have the same effect by producing possibly transient diffusion channels [92], such that the rapid (several seconds) diffusion of a fraction of complexes out of the grana stack would be possible. This has been experimentally observed by fluorescence recovery after photobleaching (FRAP) experiments [96,97]. These studies illustrate the insight that can be obtained by using simulations to help unravel the physical details behind processes that would otherwise be difficult to explain.

4.3. Structural studies of extrinsic subunits and quinone binding sites

Returning to where we started in this review, homology modelling based on the bacterial reaction centre was relied on in the early days of computational studies of PSII to build model structures of PSII. Even though crystal structures of PSII are now available, homology models and related structural studies remain valuable tools in elucidating other aspects of PSII function. The investigation of the extrinsic subunits is such an example.

Extrinsic subunits on the luminal side of PSII are found across all PSII-containing organisms, and they have been shown to be important for stabilisation of the OEC, as well as assembly and repair of PSII [98]. However, while the available crystal structures of PSII do show the presence of three of these subunits (PsbO, PsbU, PsbV), there are still important gaps in our knowledge. To begin with, the positions and interactions of these subunits in the crystal structure do not necessarily apply to all PSII-containing organisms. This is because the number and identity of these small subunits vary across the different families of photosynthetic organisms [99,100]. While PsbO is ubiquitous in all families of PSII-containing organisms (red algae, green algae, cyanobacteria, plants), PsbU and PsbV are only found in cyanobacteria (e.g., *T. elongatus* and *T. vulcanus*, from which the PSII structures were obtained) and red algae. By contrast, while two other extrinsic subunits (PsbP, PsbQ) are present in all these families of organisms (except PsbP, which is not present in red algae), neither of these subunits were found in the (cyanobacterial) PSII crystal structures, possibly due to their being lost during the crystallisation procedure. Crystal structures of isolated PsbP and PsbQ from both cyanobacteria and higher plants have been successfully solved [101–104], but the same is not true for the PsbO subunit, for which only the cyanobacterial structure is known [2,3].

Against this backdrop, computational studies can provide valuable information to complement experimental studies. It has been recently shown that despite the low degree of sequence identity between cyanobacterial and plant PsbP (~24%) [102], their crystal structures show very similar tertiary structures. The same has been found for PsbQ, which is also poorly conserved across cyanobacteria and plants [104]. Molecular modelling of the surfaces and electrostatics of these subunits have allowed the comparisons of the cyanobacterial and plant forms of these subunits [102,104]. In conjunction with other literature biochemical studies, the modelling has provided clues about structural features that are important to their function [105]. In the case of PsbO, where sequence identity between the cyanobacterial and plant forms is also only moderate (~40–50%), analogous homology modelling techniques and analyses of the resulting structures have been used to increase understanding of this important subunit [106–108]. The low sequence identity but high structural similarities between the different forms of each of these extrinsic subunits may actually help future computational studies. By reducing the number of possible regions of interest to conserved regions, it may be easier to pinpoint residues and/or structural features that are critical to the functions of these subunits. Furthermore, these subunits would appear to be prime candidates for further studies using other computational techniques such as QM, MM and MD.

Finally, another area worth mentioning where computational studies have led to interesting insights at a molecular level is the study of herbicide binding in the Q_B pocket of PSII. Various molecules such as DCMU, bromoxynil and atrazine can bind to the Q_B site and block forward electron transfer from Q_A[109]. It has also been shown that these compounds can lead to changes in the midpoint potential of the Q_A/Q_A^- couple, which may be relevant to both photoprotection and photodamage mechanisms in PSII [110–112]. In order to understand how these and other PSII inhibitors bind to the Q_B pocket, computational docking calculations were recently used by Takahashi et al. [113] to study the docking of plastoquinone, DCMU and bromoxynil. DFT calculations were then used to obtain simulated FT-IR spectra, which were then compared to experimental data. This gave information about the protonation state of bromoxynil when bound to the Q_B pocket, its conformation and the hydrogen bonding interactions with the surrounding residues, as well as possible consequences of this for the Q_A/Q_A^- potential. Computational homology modelling and docking were also used by Giardi and co-workers [114,115] to select mutation sites at the Q_B pocket sites that would generate *Chlamydomonas reinhardtii* mutants with enhanced affinity for triazine and urea-type herbicides. The best candidates (D1-S268C and -S264K) were then constructed in vivo, and the increased affinity was shown by variable fluorescence measurements. The potential of these mutants in whole-cell biosensor applications was also demonstrated.

5. Concluding remarks

There is as yet much to be discovered about how PSII catalyses the water oxidation reaction under a range of physiological conditions.

Experimental studies continue to provide more and more details about the reactions that take place, and the features of this enzyme that enable it to do so. Complementary to this, computational studies can provide us not only with a more detailed understanding of what goes on, but also how and why it happens the way it does. They can also provide information at an energetic, physical and molecular level that gives us an ever better understanding of the processes that take place. The studies reviewed in this article are no doubt only the beginning of many investigations that will with time allow us to unlock the mysteries surrounding this remarkable enzyme.

6. Note added in proof

Y. Umena, K. Kawakami, J.-R. Shen, N Kamiya, Crystal structure of oxygen-evolving photosystem II at a resolution of 1.9 Å, Nature 473 (2011) 55-60.

Acknowledgements

The financial support of the Carl Tryggers Foundation for Scientific Research, the Knut and Alice Wallenberg Foundation, the EU Solar-H2 network, the Swedish Energy Agency and the Swedish Research Council is gratefully acknowledged.

References

[1] J. Yano, J. Kern, K.D. Irrgang, M.J. Latimer, U. Bergmann, P. Glatzel, Y. Pushkar, J. Biesiadka, B. Loll, K. Sauer, J. Messinger, A. Zouni, V.K. Yachandra, X-ray damage to the Mn_4Ca complex in single crystals of photosystem II: a case study for metalloprotein crystallography, Proc. Natl. Acad. Sci. U. S. A. 102 (2005) 12047–12052.
[2] K.N. Ferreira, T.M. Iverson, K. Maghlaoui, J. Barber, S. Iwata, Architecture of the photosynthetic oxygen-evolving center, Science 303 (2004) 1831–1838.
[3] B. Loll, J. Kern, W. Saenger, A. Zouni, J. Biesiadka, Towards complete cofactor arrangement in the 3.0 angstrom resolution structure of photosystem II, Nature 438 (2005) 1040–1044.
[4] A. Guskov, J. Kern, A. Gabdulkhakov, M. Broser, A. Zouni, W. Saenger, Cyanobacterial photosystem II at 2.9-angstrom resolution and the role of quinones, lipids, channels and chloride, Nat. Struct. Mol. Biol. 16 (2009) 334–342.
[5] T.J. Wydrzynski, K. Satoh (Eds.), Photosystem II: the light-driven water: plastoquinone oxidoreductase, Springer, The Netherlands, 2005.
[6] T.J. Aartsma, J. Matysik (Eds.), Biophysical Techniques in Photosynthesis, Springer, The Netherlands, 2008.
[7] B. Svensson, I. Vass, E. Cedergren, S. Styring, Structure of donor side components in photosystem II predicted by computer modeling, EMBO J. 9 (1990) 2051–2059.
[8] B. Svensson, I. Vass, S. Styring, Sequence-analysis of the D1 and D2 reaction center proteins of photosystem II, Z. Naturforsch. C 46 (1991) 765–776.
[9] K.G. Tietjen, J.F. Kluth, R. Andree, M. Haug, M. Lindig, K.H. Muller, H.J. Wroblowsky, A. Trebst, The herbicide binding niche of photosystem-II—a model, Pestic. Sci. 31 (1991) 65–72.
[10] S.V. Ruffle, D. Donnelly, T.L. Blundell, J.H.A. Nugent, A three-dimensional model of the photosystem II reaction center of *Pisum sativum*, Photosynth. Res. 34 (1992) 287–300.
[11] U. Egner, G.A. Hoyer, W. Saenger, Modeling and energy minimization studies on the herbicide binding-protein (D1) in photosystem-II of plants, Biochim. Biophys. Acta 1142 (1993) 106–114.
[12] B. Svensson, C. Etchebest, P. Tuffery, P. vanKan, J. Smith, S. Styring, A model for the photosystem II reaction center core including the structure of the primary donor P-680, Biochemistry 35 (1996) 14486–14502.
[13] H. Dau, M. Haumann, The manganese complex of photosystem II in its reaction cycle - Basic framework and possible realization at the atomic level, Coord. Chem. Rev. 252 (2008) 273–295.
[14] M. Haumann, P. Liebisch, C. Muller, M. Barra, M. Grabolle, H. Dau, Photosynthetic O_2 formation tracked by time-resolved X-ray experiments, Science 310 (2005) 1019–1021.
[15] J. Messinger, J.H. Robblee, U. Bergmann, C. Fernandez, P. Glatzel, H. Visser, R.M. Cinco, K.L. McFarlane, E. Bellacchio, S.A. Pizarro, S.P. Cramer, K. Sauer, M.P. Klein, V.K. Yachandra, Absence of Mn-centered oxidation in the S-2 ->S-3 transition: implications for the mechanism of photosynthetic water oxidation, J. Am. Chem. Soc. 123 (2001) 7804–7820.
[16] J. Yano, J. Kern, K. Sauer, M.J. Latimer, Y. Pushkar, J. Biesiadka, B. Loll, W. Saenger, J. Messinger, A. Zouni, V.K. Yachandra, Where water is oxidized to dioxygen: structure of the photosynthetic Mn4Ca cluster, Science 314 (2006) 821–825.
[17] J. Yano, V.K. Yachandra, Where water is oxidized to dioxygen: structure of the photosynthetic Mn4Ca cluster from X-ray spectroscopy, Inorg. Chem. 47 (2008) 1711–1726.
[18] A.R. Leach, Molecular modelling: principles and applications, 2nd ed. Prentice Hall, Harlow, 2001.
[19] S.F. Sousa, P.A. Fernandes, M.J. Ramos, General performance of density functionals, J. Phys. Chem. A 111 (2007) 10439–10452.
[20] P.E.M. Siegbahn, R.H. Crabtree, Manganese oxyl radical intermediates and O—O bond formation in photosynthetic oxygen evolution and a proposed role for the calcium cofactor in photosystem II, J. Am. Chem. Soc. 121 (1999) 117–127.
[21] P.E.M. Siegbahn, Theoretical models for the oxygen radical mechanism of water oxidation and of the water oxidizing complex of photosystem II, Inorg. Chem. 39 (2000) 2923–2935.
[22] M. Lundberg, P.E.M. Siegbahn, Theoretical investigations of structure and mechanism of the oxygen-evolving complex in PSII, Phys. Chem. Chem. Phys. 6 (2004) 4772–4780.
[23] M. Lundberg, P.E.M. Siegbahn, Minimum energy spin crossings for an O—O bond formation reaction, Chem. Phys. Lett. 401 (2005) 347–351.
[24] P.E.M. Siegbahn, M. Lundberg, The mechanism for dioxygen formation in PSII studied by quantum chemical methods, Photochem. Photobiol. Sci. 4 (2005) 1035–1043.
[25] P.E.M. Siegbahn, O—O bond formation in the S_4 state of the oxygen-evolving complex in photosystem II, Chem. Eur. J. 12 (2006) 9217–9227.
[26] E.M. Siegbahn, A structure-consistent mechanism for dioxygen formation in photosystem II, Chem. Eur. J. 14 (2008) 8290–8302.
[27] P.E.M. Siegbahn, Theoretical studies of O—O bond formation in photosystem II, Inorg. Chem. 47 (2008) 1779–1786.
[28] P.E.M. Siegbahn, Mechanism and energy diagram for O—O bond formation in the oxygen-evolving complex in photosystem II, Philos. Trans. R. Soc. B Biol. Sci. 363 (2008) 1221–1228.
[29] P.E.M. Siegbahn, An energetic comparison of different models for the oxygen evolving complex of photosystem II, J. Am. Chem. Soc. 131 (2009) 18238–18239.
[30] P.E.M. Siegbahn, Structures and energetics for O_2 formation in photosystem II, Acc. Chem. Res. 42 (2009) 1871–1880.
[31] P.E.M. Siegbahn, Water oxidation in photosystem II: oxygen release, proton release and the effect of chloride, Dalton Trans. (2009) 10063–10068.
[32] M.R.A. Blomberg, P.E.M. Siegbahn, Quantum chemistry as a tool in bioenergetics, Biochim. Biophys. Acta 1797 (2010) 129–142.
[33] P.E.M. Siegbahn, T. Borowski, Modeling enzymatic reactions involving transition metals, Acc. Chem. Res. 39 (2006) 729–738.
[34] M. Haumann, C. Muller, P. Liebisch, L. Iuzzolino, J. Dittmer, M. Grabolle, T. Neisius, W. Meyer-Klaucke, H. Dau, Structural and oxidation state changes of the photosystem II manganese complex in four transitions of the water oxidation cycle ($S_0 \rightarrow S_1$, $S_1 \rightarrow S_2$, $S_2 \rightarrow S_3$, and $S_3,S_4 \rightarrow S_0$) Characterized by X-ray absorption spectroscopy at 20 K and room temperature, Biochemistry 44 (2005) 1894–1908.
[35] P.E.M. Siegbahn, The performance of hybrid DFT for mechanisms involving transition metal complexes in enzymes, J. Biol. Inorg. Chem. 11 (2006) 695–701.
[36] E.M. Sproviero, J.A. Gascon, J.P. McEvoy, G.W. Brudvig, V.S. Batista, QM/MM models of the O_2-evolving complex of photosystem II, J. Chem. Theory Comput. 2 (2006) 1119–1134.
[37] E.M. Sproviero, J.A. Gascon, J.P. McEvoy, G.W. Brudvig, V.S. Batista, Characterization of synthetic oxomanganese complexes and the inorganic core of the O-2-evolving complex in photosystem—II: evaluation of the DFT/B3LYP level of theory, J. Inorg. Biochem. 100 (2006) 786–800.
[38] V. Batista, E. Sproviero, J. Gascon, J. McEvoy, G. Brudvig, DFT-QM/MM structural models of the oxygen-evolving complex of photosystem II, Photosynth. Res. 91 (2007) 173.
[39] E.M. Sproviero, J.A. Gascon, J.P. McEvoy, G.W. Brudvig, V.S. Batista, Quantum mechanics/molecular mechanics structural models of the oxygen-evolving complex of photosystem II, Curr. Opin. Struct. Biol. 17 (2007) 173–180.
[40] E.M. Sproviero, J.A. Gascon, J.P. McEvoy, G.W. Brudvig, V.S. Batista, Quantum mechanics/molecular mechanics study of the catalytic cycle of water splitting in photosystem II, J. Am. Chem. Soc. 130 (2008) 3428–3442.
[41] E.M. Sproviero, J.A. Gascon, J.P. McEvoy, G.W. Brudvig, V.S. Batista, Computational studies of the O_2-evolving complex of photosystem II and biomimetic oxomanganese complexes, Coord. Chem. Rev. 252 (2008) 395–415.
[42] E.M. Sproviero, J.A. Gascon, J.P. McEvoy, G.W. Brudvig, V.S. Batista, A model of the oxygen-evolving center of photosystem II predicted by structural refinement based on EXAFS simulations, J. Am. Chem. Soc. 130 (2008) 6728–6730.
[43] E.M. Sproviero, J.P. McEvoy, J.A. Gascon, G.W. Brudvig, V.S. Batista, Computational insights into the O_2-evolving complex of photosystem II, Photosynth. Res. 97 (2008) 91–114.
[44] E.M. Sproviero, K. Shinopoulos, J.A. Gascon, J.P. McEvoyO, G.W. Brudvig, V.S. Batista, QM/MM computational studies of substrate water binding to the oxygen-evolving centre of photosystem II, Philos. Trans. R. Soc. B Biol. Sci. 363 (2008) 1149–1156.
[45] M. Svensson, S. Humbel, R.D.J. Froese, T. Matsubara, S. Sieber, K. Morokuma, ONIOM: a multilayered integrated MO + MM method for geometry optimizations and single point energy predictions. A test for Diels-Alder reactions and Pt(P(t-Bu)(3))(2) + H-2 oxidative addition, J. Phys. Chem. 100 (1996) 19357–19363.
[46] R. Zhang, B. Lev, J.E. Cuervo, S.Y. Noskov, D.R. Salahub, A Guide to QM/MM Methodology and Applications, Advances in Quantum Chemistry, vol. 59, Elsevier Academic Press Inc., San Diego, 2010, pp. 353–400.
[47] R.J. Debus, M.A. Strickler, L.M. Walker, W. Hillier, No evidence from FTIR difference spectroscopy that aspartate-170 of the D1 polypeptide ligates a manganese ion that undergoes oxidation during the S-0 to S-1, S-1 to S-2, or S-2 to S-3 transitions in photosystem II, Biochemistry 44 (2005) 1367–1374.
[48] J.S. Vrettos, J. Limburg, G.W. Brudvig, Mechanism of photosynthetic water oxidation: combining biophysical studies of photosystem II with inorganic model chemistry, Biochim. Biophys. Acta 1503 (2001) 229–245.

[49] V.L. Pecoraro, M.J. Baldwin, M.T. Caudle, W.Y. Hsieh, N.A. Law, A proposal for water oxidation in photosystem II, Pure Appl. Chem. 70 (1998) 925–929.
[50] J.P. McEvoy, J.A. Gascon, V.S. Batista, G.W. Brudvig, The mechanism of photosynthetic water splitting, Photochem. Photobiol. Sci. 4 (2005) 940–949.
[51] J.P. McEvoy, G.W. Brudvig, Structure-based mechanism of photosynthetic water oxidation, Phys. Chem. Chem. Phys. 6 (2004) 4754–4763.
[52] W. Hillier, T. Wydrzynski, Substrate water interactions within the photosystem II oxygen evolving complex, Phys. Chem. Chem. Phys. 6 (2004) 4882–4889.
[53] M. Orio, D.A. Pantazis, F. Neese, Density functional theory, Photosynth. Res. 102 (2009) 443–453.
[54] S. Petrie, R. Stranger, DFT and metal-metal bonding: a dys-functional treatment for multiply charged complexes? Inorg. Chem. 43 (2004) 2597–2610.
[55] D.A. Pantazis, M. Orio, T. Petrenko, S. Zein, W. Lubitz, J. Messinger, F. Neese, Structure of the oxygen-evolving complex of photosystem II: information on the S-2 state through quantum chemical calculation of its magnetic properties, Phys. Chem. Chem. Phys. 11 (2009) 6788–6798.
[56] J.W. Murray, J. Barber, Structural characteristics of channels and pathways in photosystem II including the identification of an oxygen channel, J. Struct. Biol. 159 (2007) 228–237.
[57] F.M. Ho, S. Styring, Access channels and methanol binding site to the CaMn4 cluster in photosystem II based on solvent accessibility simulations, with implications for substrate water access, Biochim. Biophys. Acta 1777 (2008) 140–153.
[58] A. Gabdulkhakov, A. Guskov, M. Broser, J. Kern, F. Muh, W. Saenger, A. Zouni, Probing the accessibility of the Mn_4Ca cluster in photosystem II: channels calculation, noble gas derivatization, and cocrystallization with DMSO, Structure 17 (2009) 1223–1234.
[59] T. Wydrzynski, W. Hillier, J. Messinger, On the functional significance of substrate accessibility in the photosynthetic water oxidation mechanism, Physiol. Plant. 96 (1996) 342–350.
[60] J.M. Anderson, Does functional photosystem II complex have an oxygen channel? FEBS Lett. 488 (2001) 1–4.
[61] F.M. Ho, Uncovering channels in photosystem II by computer modelling: current progress, future prospects, and lessons from analogous systems, Photosynth. Res. 98 (2008) 503–522.
[62] M. Petřek, M. Otyepka, P. Banáš, P. Košinová, J. Koča, J. Damborský, CAVER: a new tool to explore routes from protein clefts, pockets and cavities, BMC Bioinformatics 7 (2006).
[63] R.J. Debus, The catalytic manganese cluster: protein ligation, in: T. Wydrzynski, K. Satoh (Eds.), Photosystem II: the light-driven water:plastoquinone oxidoreductase, Springer, The Netherlands, 2005, pp. 261–284.
[64] C. Tommos, Electron, proton and hydrogen-atom transfers in photosynthetic water oxidation, Philos. Trans. R. Soc. Lond. B Biol. Sci. 357 (2002) 1383–1394.
[65] S. Vassiliev, P. Comte, A. Mahboob, D. Bruce, Tracking the flow of water through photosystem II using molecular dynamics and streamline tracing, Biochemistry 49 (2010) 1873–1881.
[66] H. Johansen-Berg, M.F.S. Rushworth, Using diffusion imaging to study human connectional anatomy, Annu. Rev. Neurosci. 32 (2009) 75–94.
[67] J.W. Murray, K. Maghlaoui, J. Kargul, M. Sugiura, J. Barber, Analysis of xenon binding to photosystem II by X-ray crystallography, Photosynth. Res. 98 (2008) 523–527.
[68] C.J.T.V. Grotthuss, Sur la decomposition de l'eau et des corps qu'elle tient en dissolution a l'aide de l'électricité galvanique, Ann. Chim. 58 (1806) 54–74.
[69] S. Cukierman, Et tu, Grotthuss! and other unfinished stories, Biochim. Biophys. Acta 1757 (2006) 876–885.
[70] J.M.J. Swanson, C.M. Maupin, H.N. Chen, M.K. Petersen, J.C. Xu, Y.J. Wu, G.A. Voth, Proton solvation and transport in aqueous and biomolecular systems: insights from computer simulations, J. Phys. Chem. B 111 (2007) 4300–4314.
[71] C.A. Wraight, Chance and design—proton transfer in water, channels and bioenergetic proteins, Biochim. Biophys. Acta 1757 (2006) 886–912.
[72] J. Barber, K. Ferreira, K. Maghlaoui, S. Iwata, Structural model of the oxygen-evolving centre of photosystem II with mechanistic implications, Phys. Chem. Chem. Phys. 6 (2004) 4737–4742.
[73] H. Ishikita, W. Saenger, B. Loll, J. Biesiadka, E.W. Knapp, Energetics of a possible proton exit pathway for water oxidation in photosystem II, Biochemistry 45 (2006) 2063–2071.
[74] H.A. Chu, A.P. Nguyen, R.J. Debus, Amino acid residues that influence the binding of manganese or calcium to photosystem-II.1. The lumenal interhelical domains of the D1 polypeptide, Biochemistry 34 (1995) 5839–5858.
[75] J.M.J. Swanson, J. Simons, Role of charge transfer in the structure and dynamics of the hydrated proton, J. Phys. Chem. B 113 (2009) 5149–5161.
[76] F.M. Ho, Molecular Dynamics Simulations of a Putative H^+ Pathway in Photosystem II, Proceedings of the 15th International Congress of Photosynthesis, Beijing, China. (in press).
[77] Z.L. Li, R.L. Burnap, Mutations of basic arginine residue 334 in the D1 protein of photosystem II lead to unusual S-2 state properties in Synechocystis sp PCC 6803, Photosynth. Res. 72 (2002) 191–201.
[78] R. van Grondelle, V.I. Novoderezhkin, J.P. Dekker, Modeling light harvesting and primary charge separation in photosystem I and photosystem II, in: A. Laisk, L. Nedbal, Govindjee (Eds.), Photosynthesis *in silico*: understanding complexity from molecules to ecosystems, vol. 29, Springer, The Netherlands, 2009, pp. 33–53.
[79] T. Renger, A.R. Holzwarth, Theory of excitation energy transfer and optical spectra of photosynthetic systems, in: T.J. Aartsma, J. Matysik (Eds.), Biophysical Techniques in Photosynthesis, vol. 26, Springer, The Netherlands, 2008, pp. 421–443.
[80] Y.C. Cheng, G.R. Fleming, Dynamics of light harvesting in photosynthesis, Annu. Rev. Phys. Chem. 60 (2009) 241–262.
[81] J. Neugebauer, Subsystem-based theoretical spectroscopy of biomolecules and biomolecular assemblies, Chemphyschem 10 (2009) 3148–3173.
[82] V.I. Novoderezhkin, R. van Grondelle, Physical origins and models of energy transfer in photosynthetic light-harvesting, Phys. Chem. Chem. Phys. 12 (2010) 7352–7365.
[83] T. Renger, E. Schlodder, Primary photophysical processes in photosystem II: bridging the gap between crystal structure and optical spectra, Chemphyschem 11 (2010) 1141–1153.
[84] S. Vasil'ev, D. Bruce, A protein dynamics study of photosystem II: the effects of protein conformation on reaction center function, Biophys. J. 90 (2006) 3062–3073.
[85] C.C. Moser, C.C. Page, R. Farid, P.L. Dutton, Biological electron-transfer, J. Bioenerg. Biomembr. 27 (1995) 263–274.
[86] I.P. Mercer, I.R. Gould, D.R. Klug, A quantum mechanical/molecular mechanical approach to relaxation dynamics: calculation of the optical properties of solvated bacteriochlorophyll-a, J. Phys. Chem. B 103 (1999) 7720–7727.
[87] A. Damjanovic, I. Kosztin, U. Kleinekathofer, K. Schulten, Excitons in a photosynthetic light-harvesting system: a combined molecular dynamics, quantum chemistry, and polaron model study, Phys. Rev. E 65 (2002) 031919.
[88] L. Janosi, I. Kosztin, A. Damjanovic, Theoretical prediction of spectral and optical properties of bacteriochlorophylls in thermally disordered LH2 antenna complexes, J. Chem. Phys. 125 (2006) 014903.
[89] H. Kirchhoff, U. Mukherjee, H.J. Galla, Molecular architecture of the thylakoid membrane: lipid diffusion space for plastoquinone, Biochemistry 41 (2002) 4872–4882.
[90] E.M. Aro, I. Virgin, B. Andersson, Photoinhibition of photosystem-2—inactivation, protein damage and turnover, Biochim. Biophys. Acta 1143 (1993) 113–134.
[91] R. Danielsson, M. Suorsa, V. Paakkarinen, P.A. Albertsson, S. Styring, E.M. Aro, F. Mamedov, Dimeric and monomeric organization of photosystem II - Distribution of five distinct complexes in the different domains of the thylakoid membrane, J. Biol. Chem. 281 (2006) 14241–14249.
[92] H. Kirchhoff, I. Tremmel, W. Haase, U. Kubitscheck, Supramolecular photosystem II organization in grana thylakoid membranes: evidence for a structured affangement, Biochemistry 43 (2004) 9204–9213.
[93] H. Kirchhoff, Molecular crowding and order in photosynthetic membranes, Trends Plant Sci. 13 (2008) 201–207.
[94] I.G. Tremmel, H. Kirchhoff, E. Weis, G.D. Farquhar, Dependence of plastoquinol diffusion on the shape, size, and density of integral thylakoid proteins, Biochim. Biophys. Acta 1607 (2003) 97–109.
[95] H. Kirchhoff, S. Lenhert, C. Buchel, L. Chi, J. Nield, Probing the organization of photosystem II in photosynthetic membranes by atomic force microscopy, Biochemistry 47 (2008) 431–440.
[96] H. Kirchhoff, S. Haferkamp, J.F. Allen, D.B.A. Epstein, C.W. Mullineaux, Protein diffusion and macromolecular crowding in thylakoid membranes, Plant Physiol. 146 (2008) 1571–1578.
[97] C.W. Mullineaux, Factors controlling the mobility of photosynthetic proteins, Photochem. Photobiol. 84 (2008) 1310–1316.
[98] P.J. Nixon, F. Michoux, J.F. Yu, M. Boehm, J. Komenda, Recent advances in understanding the assembly and repair of photosystem II, Ann. Bot. 106 (2010) 1–16.
[99] J.L. Roose, K.M. Wegener, H.B. Pakrasi, The extrinsic proteins of photosystem II, Photosynth. Res. 92 (2007) 369–387.
[100] K. Ifuku, S. Ishihara, F. Sato, Molecular functions of oxygen-evolving complex family proteins in photosynthetic electron flow, J. Integr. Plant Biol. 52 (2010) 723–734.
[101] K. Ifuku, T. Nakatsu, H. Kato, F. Sato, Crystal structure of the PsbP protein of photosystem II from Nicotiana tabacum, EMBO Rep. 5 (2004) 362–367.
[102] F. Michoux, K. Takasaka, M. Boehm, P.J. Nixon, J.W. Murray, Structure of CyanoP at 2.8 angstrom: implications for the evolution and function of the PsbP subunit of photosystem II, Biochemistry 49 (2010) 7411–7413.
[103] M. Balsera, J.B. Arellano, J.L. Revuelta, J. de las Rivas, J.A. Hermoso, The 1.49 angstrom resolution crystal structure of PsbQ from photosystem II of Spinacia oleracea reveals a PPII structure in the N-terminal region, J. Mol. Biol. 350 (2005) 1051–1060.
[104] S.A. Jackson, R.D. Fagerlund, S.M. Wilbanks, J.J. Eaton-Rye, Crystal structure of PsbQ from Synechocystis sp PCC 6803 at 1.8 angstrom: implications for binding and function in cyanobacterial photosystem II, Biochemistry 49 (2010) 2765–2767.
[105] K. Ifuku, S. Ishihara, R. Shimamoto, K. Ido, F. Sato, Structure, function, and evolution of the PsbP protein family in higher plants, Photosynth. Res. 98 (2008) 427–437.
[106] J. De Las Rivas, J. Barber, Analysis of the structure of the PsbO protein and its implications, Photosynth. Res. 81 (2004) 329–343.
[107] A.K. Williamson, J.R. Liggins, W. Hillier, T. Wydrzynski, The importance of protein–protein interactions for optimising oxygen activity in photosystem II: reconstitution with a recombinant thioredoxin–manganese stabilising protein, Photosynth. Res. 92 (2007) 305–314.
[108] H. Popelkova, A. Commet, C.F. Yocum, Asp157 is required for the function of PsbO, the photosystem II manganese stabilizing protein, Biochemistry 48 (2009) 11920–11928.
[109] A. Trebst, Inhibitors in the functional dissection of the photosynthetic electron transport system, Photosynth. Res. 92 (2007) 217–224.
[110] A. Krieger-Liszkay, A.W. Rutherford, Influence of herbicide binding on the redox potential of the quinone acceptor in photosystem—II. Relevance to photodamage and phytotoxicity, Biochemistry 37 (1998) 17339–17344.
[111] A. Krieger-Liszkay, C. Fufezan, A. Trebst, Singlet oxygen production in photosystem II and related protection mechanism, Photosynth. Res. 98 (2008) 551–564.

[112] I. Vass, K. Cser, Janus-faced charge recombinations in photosystem II photoinhibition, Trends Plant Sci. 14 (2009) 200–205.
[113] R. Takahashi, K. Hasegawa, A. Takano, T. Noguchi, Structures and binding sites of phenolic herbicides in the Q(B) pocket of photosystem II, Biochemistry 49 (2010) 5445–5454.
[114] G. Rea, F. Polticelli, A. Antonacci, V. Scognamiglio, P. Katiyar, S.A. Kulkarni, U. Johanningmeier, M.T. Giardi, Structure-based design of novel Chlamydomonas reinhardtii D1-D2 photosynthetic proteins for herbicide monitoring, Protein Sci. 18 (2009) 2139–2151.
[115] M.T. Giardi, V. Scognamiglio, G. Rea, G. Rodio, A. Antonacci, M. Lambreva, G. Pezzotti, U. Johanningmeier, Optical biosensors for environmental monitoring based on computational and biotechnological tools for engineering the photosynthetic D1 protein of Chlamydomonas reinhardtii, Biosens. Bioelectron. 25 (2009) 294–300.